Atmos. Chem. Phys. Discuss., doi:10.5194/acp-2016-167, 2016
Manuscript under review for journal Atmos. Chem. Phys.
Published: 1 April 2016

Atmospheric Chemistry and Physics Discussions
Open Access

Impacts of Global Wildfire Aerosols on Direct Radiative, Cloud and Surface-Albedo Effects Simulated with CAM5

Yiquan Jiang[1,2], Zheng Lu[2], Xiaohong Liu[2,*], Yun Qian[3], Kai Zhang[3], Yuhang Wang[4] and Xiu-Qun Yang[1]

[1] *CMA-NJU Joint Laboratory for Climate Prediction Studies, Institute for Climate and Global Change Research, School of Atmospheric Sciences, Nanjing University, Nanjing, China*

[2] *Department of Atmospheric Science, University of Wyoming*

[3] *Pacific Northwest National Laboratory, Richland, Washington, USA*

[4] *School of Earth and Atmospheric Sciences, Georgia Institute of Technology, Atlanta, Georgia, USA*

*Corresponding author:

Dr. Xiaohong Liu
Department of Atmospheric Science
University of Wyoming
Laramie, WY 82071
Phone (307) 766-3225
E-mail: xliu6@uwyo.edu

Atmos. Chem. Phys. Discuss., doi:10.5194/acp-2016-167, 2016
Manuscript under review for journal Atmos. Chem. Phys.
Published: 1 April 2016

Abstract

Aerosols from wild-land fires could significantly perturb the global radiation balance and induce the climate change. In this study, the Community Atmospheric Model version 5 (CAM5) with prescribed daily fire aerosol emissions is used to investigate the spatial and seasonal characteristics of radiative effects (REs) of wildfire aerosols including black carbon (BC) and particulate organic matter (POM). The global annual mean direct radiative effect (DRE) of all fire aerosols is 0.155±0.01 W m^{-2}, mainly due to the absorption of fire BC (0.25±0.01 W m^{-2}), while fire POM induces a small overall effect (-0.05 to 0.04±0.01 W m^{-2}). Strong positive DRE is found in the Arctic and in the oceanic regions west of South Africa and South America as a result of amplified absorption of fire BC above low-level clouds, in general agreement with satellite observations. The global annual mean cloud radiative effects (CRE) due to all fire aerosols is -0.70±0.05 W m^{-2}, resulting mainly from the fire POM indirect effect (-0.59±0.03 W m^{-2}). The large cloud liquid water path over land areas of the Arctic favors the strong fire aerosol indirect effect (up to -15 W m^{-2}) during the Arctic summer. Significant surface cooling, precipitation reduction and low-level cloud amount increase are also found in the Arctic summer as a result of the fire aerosol indirect effect. The global annual mean surface albedo effect (SAE) over land areas (0.03±0.10 W m^{-2}) is mainly due to the fire BC-in-snow effect (0.02 W m^{-2}) with the maximum albedo effect occurring in spring (0.12 W m^{-2}) when snow starts to melt.

Atmos. Chem. Phys. Discuss., doi:10.5194/acp-2016-167, 2016
Manuscript under review for journal Atmos. Chem. Phys.
Published: 1 April 2016

1. Introduction

Wildfires or biomass burning of living and dead vegetation are an integral component of the Earth system, and have significant impacts on the carbon cycle [*Ciais et al.*, 2013] and the climate [*Bowman et al.*, 2009; *Keywood et al.*, 2011; *Liu et al.*, 2014; *Sommers et al.*, 2014]. On one hand, wildfires can perturb the climate system by emitting greenhouse gases and aerosols [*Kaiser et al.*, 2012; *Wiedinmyer et al.*, 2011]. On the other hand, climate states and variabilities can play a critical role in determining the occurrence frequency and intensity of wildfires [*Marlon et al.*, 2009; *van der Werf et al.*, 2008; *Westerling et al.*, 2006]. However, there are still large unknowns regarding the feedback mechanisms between wildfire and climate interactions, and more investigations are needed in order to predict the future wildfire events and their climatic impacts [*Carslaw et al.*, 2010; *Liu et al.*, 2014]

Particles emitted from wildfires can exert significant perturbations to the climate system by scattering and absorbing the solar radiation in the atmosphere (i.e., direct effect) [*Carslaw et al.*, 2010] and by changing the surface albedo when they are deposited on the snow and ice (i.e., surface albedo effect) [*Flanner et al.*, 2007; *Quinn et al.*, 2008; *Randerson et al.*, 2006; *Qian et al.*, 2011, 2015]. In addition, wildfire or smoke particles can modify the cloud properties, precipitation efficiency, and the hydrological cycle by changing the atmospheric thermal structure (i.e., semi-direct effect) [*Koch and Del Genio*, 2010; *Andreae et al.*, 2004b] or acting as cloud condensation nuclei (CCN) (i.e., indirect effect) [*Andreae and Rosenfeld*, 2008; *Qian et al.*, 2009; *Lu and Sokolik*, 2013].

Atmos. Chem. Phys. Discuss., doi:10.5194/acp-2016-167, 2016
Manuscript under review for journal Atmos. Chem. Phys.
Published: 1 April 2016

The radiative effect (RE) [*Boucher and Tanre*, 2000] and radiative forcing (RF) [*Forster et al.*, 2007; *Myhre et al.*, 2013a] are typical metrics used to assess and compare anthropogenic and natural drivers of the climate change. RE represents the instantaneous radiative impact of all atmospheric particles from both anthropogenic and natural sources [*Heald et al.*, 2014]. RF is calculated as the change of RE from pre-industrial (e.g., year 1850) to present-day (e.g., year 2000) [*Heald et al.*, 2014; *Liu et al.*, 2007], based on the aerosol and precursor gas emissions in the pre-industrial and present-day times [*Dentener et al.*, 2006; *Lamarque et al.*, 2010].

The direct radiative forcing (DRF) or forcing due to Aerosol-Radiation-Interaction (ARI) of biomass burning aerosols has been estimated since the IPCC second Assessment Report (AR2). In the IPCC second and third Assessment Reports (AR2 and AR3), the DRF of biomass burning aerosols is about -0.40 W m^{-2} (ranging from -0.60 to -0.07 W m^{-2}) [*Houghton*, 1996; *McCarthy*, 2001]. In the IPCC Fourth Assessment Report (AR4), it is estimated to be about 0.03 W m^{-2} (ranging from -0.09 to 0.15 W m^{-2}) [*Forster et al.*, 2007]. The more positive forcing in the IPCC AR4 results from the improved representation of absorption properties of biomass burning aerosols and the consideration of effects of low-level clouds on the absorption of above-cloud biomass burning aerosols in the global models. Based on the Aerosol Comparisons between Observations and Models (AeroCom) Phase II simulations [*Bond et al.*, 2013; *Myhre et al.*, 2013b], the DRF of biomass burning aerosols in the IPCC Fifth Assessment Report (AR5) is estimated to be 0.0 W m^{2} (ranging from -0.20 to 0.20 W m^{-2}), and the DRFs of biomass burning black carbon

Atmos. Chem. Phys. Discuss., doi:10.5194/acp-2016-167, 2016
Manuscript under review for journal Atmos. Chem. Phys.
Published: 1 April 2016

(BC) and primary organic matter (POM) are of the opposite sign (i.e., 0.10 and -0.10 W m^{-2}, respectively).

There are also many studies that estimated the direct radiative effect (DRE) of biomass burning aerosols by comparing the simulation with fire emissions against the simulation with no fire emissions. For example, using the NCAR Community Atmosphere Model version 4 (CAM4) with a bulk aerosol module, *Tosca et al.* [2013] reported that the top-of-atmosphere (TOA) DRE from global biomass burning aerosols is 0.18 ± 0.10 W m^{-2} averaged for the period of 1997-2009. *Ward et al.* [2012] estimated the DRE from biomass burning aerosols in the pre-industrial (for the year 1850), present-day (for the year 2000), and future time periods (for the year 2100), and found that the biomass burning aerosol DRE for the year 2000 is 0.13 W m^{-2} and -0.27 W m^{-2} in all-sky and clear-sky conditions, respectively.

The cloud radiative effect (CRE) or effect due to Aerosol-Cloud-Interaction (ACI) of biomass burning aerosols can be comparable to or even larger than the DRE [*Liu et al.*, 2014]. The CRE of biomass burning aerosols was reported to be -1.16 W m^{-2} for the present day in *Chuang et al.* [2002]. With a global aerosol-climate model, the CRE of biomass burning aerosols was estimated to range from -1.74 to -1.00 W m^{-2} for the year 2000 in *Ward et al.* [2012]. The semi-direct radiative effect of biomass burning aerosols is not independently assessed in IPCC reports. The magnitude was reported to be about 7.0 W m^{-2} in the Southern American biomass burning regions by examining the radiative flux difference with and without the biomass burning aerosol effect on clouds [*Liu*, 2005].

Atmos. Chem. Phys. Discuss., doi:10.5194/acp-2016-167, 2016
Manuscript under review for journal Atmos. Chem. Phys.
Published: 1 April 2016

The radiative forcing or effect of BC from wildfires and other sources on snow and ice has been estimated in previous studies. For biomass burning emissions with a strong (1998) and weak (2001) boreal fire year, RE of fire BC-in-snow was estimated to be 0.011 and 0.006 W m^{-2}, respectively [*Flanner et al.*, 2007]. *Randerson et al.* [2006] reported that BC from a boreal forest fire deposited on snow and sea ice introduced a global annual mean RE of 8±5 W per m^2 of burned area in the first year when the fire happened. A summary of BC-in-snow forcing/effect can be found in *Bond et al*. [2013]. They reported that the present-day RE of fire BC-in-snow ranges from 0.006 to 0.02 W m^{-2} based on previous studies [*Jacobson*, 2004; *Rypdal et al.*, 2009; *Skeie et al.*, 2011; *Hansen et al.*, 2005; *Flanner et al.*, 2007, 2009; *Koch et al.*, 2009].

Biomass burning aerosols can have significant impacts on global and regional precipitation and atmospheric circulation. With the change of fire emissions from year 1860 to 2000, *Jones et al.* [2007] found that biomass burning aerosols decrease the global near-surface air temperature by about 0.25°C, when considering the feedbacks of sea surface temperature (SST) in the model. As shown in *Tosca et al.* [2013], the direct and semi-direct effects of biomass burning aerosols reduce the precipitation near the equator and weaken the Hadley circulation. With a regional climate model, *Zhang et al.* [2009] found that biomass burning aerosols may warm and stabilize the lower troposphere and thus re-enforce the dry season rainfall pattern in the Southern Amazonia. The absorption of shortwave radiation by biomass burning BC could increase the vertical stratification and inhibit both the cloud formation and

Atmos. Chem. Phys. Discuss., doi:10.5194/acp-2016-167, 2016
Manuscript under review for journal Atmos. Chem. Phys.
Published: 1 April 2016

precipitation [*Ackerman et al.*, 2000; *Tosca et al.*, 2014]. In contrast, biomass burning aerosols could invigorate the convective clouds [*Andreae et al.*, 2004a; *Koren et al.*, 2005] through suppressing warm rain processes in the convection, and enhance the latent heat release at higher levels [*Andreae and Rosenfeld*, 2008].

In this study, we estimate the present day (from year 2003 to 2011) wildfire (biomass burning) aerosol REs (DRE, CRE and SAE) using the NCAR Community Atmosphere Model version 5.3 (CAM5) with the four-mode version of the modal aerosol module (MAM4). We use two methods to calculate the DRE of biomass burning aerosols (total, BC-only, and POM-only). The spatial and seasonal characteristics of biomass burning aerosol REs, and the impacts on the global precipitation and temperature are discussed. Compared to earlier studies of biomass burning aerosol REs [*Tosca et al.*, 2013; *Ward et al.*, 2012], a number of improvements are made in this study, which include (1) a higher model horizontal resolution at 0.9° by 1.25° versus 1.9° by 2.5°, (2) the latest CAM5 model with MAM4, (3) daily instead of monthly fire emissions, and (4) a new methodology to more accurately diagnose the REs of biomass burning aerosols under the cloudy-sky condition.

The paper is organized as follows. Section 2 introduces the model and experiments. Section 3 describes the methods to diagnose the biomass burning aerosol REs. Section 4 presents the model results of biomass burning aerosol REs, and impacts on global and regional surface temperature and precipitation. Conclusions and discussion are given in Section 5.

Atmos. Chem. Phys. Discuss., doi:10.5194/acp-2016-167, 2016
Manuscript under review for journal Atmos. Chem. Phys.
Published: 1 April 2016

2. Model, Experiment Design and Aerosol Radiative Effect Method

2.1 Model

In our study, we use the Community Earth System Model (CESM) version 1.2, with the Community Atmosphere Model version 5.3 (CAM5.3) [*Neale et al.*, 2010] coupled with the Community Land Model version 4 (CLM4) [*Oleson et al.*, 2010]. The SNow, ICe, and Aerosol Radiative model (SNICAR) [*Flanner and Zender*, 2005] is turned on in the simulations to diagnose the biomass burning BC-in-snow effect. CAM5 includes several major updates in its physics parameterizations compared to previous CAM versions. A two-moment stratiform cloud microphysics scheme is included in CAM5 to predict both the mass and number mixing ratios of cloud liquid and cloud ice [*Morrison and Gettelman*, 2008]. MAM4, which was updated from the three-mode version of the Modal Aerosol Model (MAM3) [*Liu et al.*, 2012], includes aerosol mass and number mixing ratios in four lognormal modes: Aitken, accumulation, coarse, and primary carbon mode [*Liu et al.*, 2016]. The primary carbon mode is included to improve the treatment of microphysical ageing of BC and POM, compared to MAM3. MAM4 significantly increases (and improves) the near-surface BC concentrations in the Arctic with only a slight increase (~10%) in the computational time [*Liu et al.*, 2016].

2.2 Experiment design

CAM5 was run with the finite volume dynamics core in a resolution of 0.9° latitude by 1.25° longitude and 30 vertical levels. The model was run for the time

Atmos. Chem. Phys. Discuss., doi:10.5194/acp-2016-167, 2016
Manuscript under review for journal Atmos. Chem. Phys.
Published: 1 April 2016

Atmospheric Chemistry and Physics Discussions

period of year 2003 to 2011 (i.e., for 9 years) with prescribed monthly sea surface temperatures and sea ice. The year 2003 was run twice and the first year simulation was used as a model spin-up. Global Fire Emissions Database version 3.1 (GFED 3.1) daily emissions [*Giglio et al.*, 2013] for BC, POM and sulfur dioxide (SO_2) from 2003 to 2011 are prescribed, and the vertical distribution of fire emissions is based on the AeroCom protocol [*Dentener et al.*, 2006]. Anthropogenic aerosol and precursor gas emissions are from the IPCC AR5 dataset [*Lamarque et al.*, 2010]. We performed our control experiment (FIRE) with the GFED fire emissions turned on and a sensitivity experiment (NOFIRE) with the fire emissions turned off. Differences between FIRE and NOFIRE experiments are used to calculate the REs and climate effects of biomass burning aerosols. Two additional experiments (NOFIREBC and NOFIREPOM) were performed with fire BC and POM emissions turned off, respectively. Differences between the control (FIRE) and these two experiments represent the contribution from biomass burning BC and POM, respectively. Other forcings (e.g., SST, greenhouse gases) of all these experiments are kept the same. We performed ten ensemble members for each of these experiments. Furthermore, we performed the other experiment (FIRE_BBFFBF) using the modified CAM5 model that separately predicts the BC and POM from biomass burning (BB), fossil fuel (FF) and biofuel (BF) sources, while other model features are kept the same as the FIRE experiment. A summary of all the experiments in this study can be found in Table 1.

2.3 Methods of calculating fire aerosol radiative effects

Atmos. Chem. Phys. Discuss., doi:10.5194/acp-2016-167, 2016
Manuscript under review for journal Atmos. Chem. Phys.
Published: 1 April 2016

The REs of all fire aerosols, fire BC, and fire POM are calculated from the differences of TOA shortwave fluxes (ΔF) between the FIRE experiment and the three other experiments (NOFIRE, NOFIREBC and NOFIREPOM), respectively.

$$\Delta F_{\text{fire aero}} = F_{\text{fire}} - F_{\text{nofire}} \quad (1)$$

$$\Delta F_{\text{fire bc}} = F_{\text{fire}} - F_{\text{nofirebc}} \quad (2)$$

$$\Delta F_{\text{fire pom}} = F_{\text{fire}} - F_{\text{nofirepom}} \quad (3)$$

The total TOA shortwave flux change can be broken into the aerosol direct radiative effect (DRE, i.e., radiative effect from aerosol-radiation interactions), the aerosol induced cloud radiative effect (CRE, i.e., radiative effect from aerosol-cloud interactions), and the surface albedo effect (SAE, i.e., radiative effect from aerosol-surface albedo interactions). The aerosol induced CRE results from both the aerosol indirect effect on clouds via acting as CCN and the aerosol semi-direct effect on clouds via affecting the atmospheric states due to absorbing aerosols. We adopt the method of *Ghan* [2013] to separate the DRE, CRE, and SAE from the total effects of all fire aerosols, fire BC and fire POM, respectively. The method is summarized as follows. F_{clean} is the radiative flux at TOA calculated from a diagnostic radiation call in the same control simulations, but neglecting the scattering and absorption of solar radiation by aerosols. $F_{\text{clean,clear}}$ is the clear-sky radiative flux at TOA calculated from the same diagnostic radiation call, but neglecting scattering and absorption by both clouds and aerosols.

$$\Delta F = \underbrace{\Delta(F - F_{\text{clean}})}_{\text{(DRE)}} + \underbrace{\Delta(F_{\text{clean}} - F_{\text{clean,clear}})}_{\text{(CRE)}} + \underbrace{\Delta F_{\text{clean,clear}}}_{\text{(SAE)}} \quad (4)$$

Atmos. Chem. Phys. Discuss., doi:10.5194/acp-2016-167, 2016
Manuscript under review for journal Atmos. Chem. Phys.
Published: 1 April 2016

In the method above, CRE includes both aerosol indirect and semi-direct effects. The fire BC has a much weaker indirect effect due to its lower mass burden and lower hygroscopicity compared to fire POM [*Koch et al.*, 2011]. Thus the fire aerosol semi-direct effect can be approximately estimated by the CRE of fire BC. The fire aerosol indirect effect can be estimated as the difference of fire aerosol CRE and semi-direct effect.

We undertake another method to estimate the fire aerosol DRE from the experiment (FIRE_BBFFBF). With explicit predictions of fire POM and fire BC in FIRE_BBFFBF, the DREs of fire BC and fire POM are estimated by two diagnostic radiation calls, neglecting the scattering and absorption of solar radiation of fire BC and fire POM, respectively. This method is named as BBFFBF, and the DREs of fire BC and fire POM will be compared with those from the method of *Ghan* [2013]. The fire BC-in-snow effect is calculated from SNICAR, and compared with the SAE estimated from *Ghan* [2013].

3. Results

3.1 Simulation of biomass burning aerosols

The biomass burning BC and POM from forest and grass fires are significant contributors to the total BC and POM emissions. Figure 1 shows the seasonal variation of GFED fire emissions in the global, tropical (25°S to 25°N), and Arctic (60°N to 90°N) regions. Global fire emission is the largest during the boreal summer as well as in the boreal autumn (September/October), when it is the fire season in the

Atmos. Chem. Phys. Discuss., doi:10.5194/acp-2016-167, 2016
Manuscript under review for journal Atmos. Chem. Phys.
Published: 1 April 2016

tropical regions of the Southern Hemisphere (SH). The tropical fire emission contributes the most to the annual global fire emission (80% for BC and 85% for OC, respectively), compared to other regions. Arctic is the other important fire region, where the emission maximum is found during the summer. In summer, the OC emission in the Arctic regions is about 50% of that in the tropical region. The BC emission in the Arctic is much smaller than that of the tropical regions even in the summer fire season. The dominant fire type in the SH topics is deforestation, savanna and grassland fires, while that in the Arctic is the forest fires. The OC to BC ratio (OC/BC) of forest fires is almost three times higher than that of deforestation, savanna and grassland fires [*van der Werf et al.*, 2010].

Figure 2 shows the latitudinal and longitudinal distributions of vertically integrated concentrations (column burdens) of BC and POM from BB, FF, and BF sources based on the FIRE_BBFFBF experiment. The BC and POM from BB source are mainly distributed in the tropical and sub-tropical regions (South Africa, South America and Southeast Asia) and in the mid- to high latitudes (North of 45°N) of the Northern Hemisphere (NH) (Northeast Asia, Alaska and Canada). The largest column burdens of biomass burning aerosols are located in South Africa and adjacent oceanic areas (1.5 and 20 mg m^{-2} for BC and POM, respectively). The biomass burning aerosols are important aerosol species in the Arctic regions, and contribute up to 53% and 86% to the total burden of BC and POM in the Arctic (from 60° N to 90°N), respectively. In comparison, the maximum column burdens of fossil fuel BC and POM are found in East Asia, South Asia, Western Europe and North America. The

Atmos. Chem. Phys. Discuss., doi:10.5194/acp-2016-167, 2016
Manuscript under review for journal Atmos. Chem. Phys.
Published: 1 April 2016

maximum column burdens of biofuel BC and POM occur in East Asia, South Asia and Central Africa. The biofuel and fossil fuel sources are dominant contributors to BC and POM in East Asia and South Asia. In other regions of the world, biomass burning is the primary source of BC and POM. Globally, the biomass burning contributes 41% and 70% to the total burdens of BC and POM, respectively. Biomass burning can also emit SO_2. However, it only contributes ~3% to the total global sulfate burden (figure not shown), so only radiative effects of biomass burning POM and BC are discussed in this study.

The simulated aerosol optical depth (AOD) and single scattering albedo (SSA) are validated with observations from the AErosol RObotic NETwork (AERONET, http://aeronet.gsfc.nasa.gov) at sites significantly affected by biomass burning activities in South Africa, South America and the Arctic regions. The AERONET AOD and SSA data are averaged for the years from 2003 to 2011 to match the simulation period. We note that *Tosca et al.* [2013] and *Ward et al.* [2012] applied scaling factors (from 1 to 3 varying by regions) to fire emissions to improve modeled AOD magnitudes. In South Africa, modeled monthly AOD agrees with observations within a factor of 2 for the three sites (Figure 3a-3c). The underestimation of AOD is found in the tropical site (Mongu) (Figure 3a) during autumn (the fire season). The simulated AOD in the two other sites (Skukuza and Ascension Island) is generally consistent with observations in both the magnitude and seasonal trend. The simulated SSA in South Africa ranges between 0.75 and 0.95 and generally matches the observed SSA magnitude and trend in the two land sites (Mongu and Skukuza)

(Figure 4a-4b). However, an overestimation of SSA is found in the oceanic site (Ascension Island) (Figure 4c). The reason for this overestimation of SSA and thus the underestimation of absorption AOD (AAOD) is unclear and could be due to that the model has not treated the absorption enhancement of aged fire BC during its transport.

The simulated AOD in South America is generally consistent with observations within a factor of 2 (Figure 3d-3f). The seasonal variation of simulated AOD generally matches the observations. The underestimation of AOD in Alta Floresta and Cuiaba-Miranda is most obvious in September and October (the fire season), which may be attributed to the underestimation of fire emissions. The simulated SSA in South America ranges mostly between 0.87–0.95 and matches the observations reasonably well (Figure 4d-4f).

In the Arctic, small AOD (less than 0.3) and large SSA (larger than 0.9) are observed for the three sites. The large SSA in the fire season (summer) is consistent with the high OC/BC ratio of fire emissions in the Arctic (Figure 1). The model significantly underestimates the observed AOD in the Arctic in both fire and non-fire seasons. The underestimation of AOD can be due to (1) the underestimation of fire emissions in the NH high latitudes [e.g., *Stohl et al.*, 2013] and/or fossil fuel emissions in Asia [e.g., *Cohen and Wang*, 2014], (2) the excessive scavenging of aerosols during their transport from the NH mid-latitude industrial regions by liquid-phase clouds [*Wang et al.*, 2013], and (3) the coarse horizontal resolution (~100 km) of the model [*Ma et al.*, 2014]. Although MAM4 increases the column

Atmos. Chem. Phys. Discuss., doi:10.5194/acp-2016-167, 2016
Manuscript under review for journal Atmos. Chem. Phys.
Published: 1 April 2016

burdens of POM and BC by up to 40 % in many remote regions compared to MAM3, it still underestimates the surface BC concentrations in the Arctic [*Liu et al.*, 2016]. The modeled SSA in the Arctic is lower than observations, which implies that the simulation of AAOD is better than that of AOD and the underestimation of non-absorbing aerosols (e.g., sulfate) in the Arctic may be more severe than that of BC.

3.2 Direct radiative effect

The annual mean DREs of all fire aerosols (including BC, POM and sulfate), fire BC and POM, estimated with the method of BBFFBF and with the method of *Ghan* [2013] are shown in Figure 5, respectively. The fire sulfate is not included in the calculation of DRE of all fire aerosols with the method of BBFFBF. Its effect is minor since the global annual mean burden of fire sulfate (0.09 mg m^{-2}) is much smaller than that of fire POM (1.25 mg m^{-2}), both of which are light-scattering. The DRE of all fire aerosols from the two methods agree with each other very well. The global annual mean DRE of all fire aerosols is positive (0.155$\pm$0.01 W m^{-2}), which indicates a warming effect from all fire aerosols. The DRE is positive on the globe except in some land areas (e.g., South Africa, South America, Great Lakes, North Canada, and East Siberia). The maximum positive DRE is located in ocean areas west of South Africa (~5.0 W m^{-2}) and South America (~1.5 W m^{-2}). The positive DRE up to 1 W m^{-2} is found in the Arctic (60°N to 90°N). The different signs of DRE between land and ocean areas of South Africa and South America result from the differences in

Atmos. Chem. Phys. Discuss., doi:10.5194/acp-2016-167, 2016
Manuscript under review for journal Atmos. Chem. Phys.
Published: 1 April 2016

cloud fraction and cloud liquid water path (LWP) between land and ocean regions. In the fire season (August-September-October) of the tropical regions, cloud fraction and cloud LWP over the land areas (10% and 20 g m^{-2}, respectively) are much smaller than those over the adjacent ocean areas (70% and 70 g m^{-2}, respectively). The biomass burning aerosols are transported above the low-level stratocumulus clouds, and their absorption is amplified by these clouds [*Abel et al.*, 2005]. A comparison of modeled DRE in autumn (September-October-November) over the South Atlantic Ocean with satellite observations is shown in Figure 6. The observed above-cloud aerosol DRE is calculated with the method of *Zhang et al.* [2014] using the Aqua/MODIS and Terra/MODIS products, respectively. The observed above-cloud aerosol DRE over southeastern Atlantic Ocean is 3-12 W m^{-2}, with higher values near the coasts. The simulated DRE agrees better with Terra/MODIS observed DRE than with Aqua/MODIS in both the magnitude and spatial pattern.

The seasonal variation of DRE of all fire aerosols is shown in Figure 7. The DRE has a maximum (1.13 W m^{-2}) in the boreal summer (June-July-August, JJA) over the NH high latitudes. The maximum positive DRE in the tropical regions occurs in the summer and autumn (September, October and November, SON) during the fire season of South Africa and South America. The DRE reaches a positive maximum in Southeast Asia during the fire season in March, April and May (MAM).

The DRE of fire BC is shown in Figure 5c-5d. The fire BC DRE calculated from the two methods are similar in magnitudes and spatial patterns, and there are much less noises from the BBFFBF method. The global annual mean fire BC DRE is about

Atmos. Chem. Phys. Discuss., doi:10.5194/acp-2016-167, 2016
Manuscript under review for journal Atmos. Chem. Phys.
Published: 1 April 2016

0.25±0.01 W m^{-2} and positive over the globe (the regions with negative values in Figure 5d are in general not statistically significant). Unlike all fire aerosols, fire BC generates a positive forcing in the land regions of South Africa and South America, and the amplification effect of low-level clouds on fire BC positive forcing can be clearly seen in South Africa and adjacent Atlantic Ocean.

The global annual mean DRE of fire POM from the two methods somewhat differs from each other (Figure 5e-5f). The BBFFBF method gives a small negative value (-0.05 W m^{-2}), while the *Ghan* [2013] method shows a small positive value (0.04±0.01 W m^{-2}). The difference is mainly in the Arctic regions where the positive forcing from *Ghan* [2013] is larger than that from the BBFFBF method. This is because the removal of fire POM emissions in the NOFIREPOM experiment affects the burden of co-emitted fire BC, causing the decrease of BC burden in the Arctic (by ~0.05 mg m^{-2}) compared to the FIRE experiment. Thus, it should be careful in using the *Ghan* [2013] method to diagnose the radiative forcing of a single component within co-emitted aerosols. The DRE of fire POM is negative in most of the global regions. However, positive forcing can be found over oceanic regions west of South Africa and South America, North Pacific Ocean and the Polar regions where large amount of low-level clouds, sea ice or land ice exist. The multiple scatterings between the above-cloud fire POM and low-level clouds or between the fire POM and the Earth's bright surface with high albedos could reduce the amount of solar radiation reflected by these low-level clouds and bright surface in the case without the fire POM. With the BBFFBF method the sum of DRE from fire POM and fire BC (i.e.,

Atmos. Chem. Phys. Discuss., doi:10.5194/acp-2016-167, 2016
Manuscript under review for journal Atmos. Chem. Phys.
Published: 1 April 2016

0.20 W m^{-2}) is larger than that of all fire aerosols (0.15 W m^{-2}). It reflects the nonlinear interactions among different aerosol components [*Ghan* et al., 2012]. The nonlinearity is stronger with the *Ghan* [2013] method. The reason is that removing the emission of one species (e.g., fire POM in the NOFIREPOM experiment) can affect the burden of other co-emitted species (e.g., fire BC).

3.3 Cloud radiative effect

The annual mean CREs due to all fire aerosols, fire BC, and fire POM are shown in Figure 8. The CRE diagnosed with the *Ghan* [2013] method includes both aerosol indirect and semi-direct effects. The fire aerosol semi-direct effect (to be discussed below) is much smaller (-0.04±0.03 W m^{-2} on the global mean) than the indirect effect, and the CRE is mostly from the fire aerosol indirect effect. The global annual mean CRE of all fire aerosols is -0.70±0.05 W m^{-2}. In the tropical regions, the strong negative CRE is located in the adjacent ocean areas of South Africa, South America and Australia, with the maximum CRE of -8.0 W m^{-2} over the South Atlantic Ocean. The strong negative fire aerosol CRE also occurs in the Arctic (60°N to 90°N). The CRE in East Siberia, Alaska and Canada is as large as -6.0 W m^{-2}.

The fire BC has a weak indirect effect by acting as CCN, but can reduce the cloud amount through its semi-direct effect. The CRE of fire BC (Figure 8b) can approximate the fire BC semi-direct effect with a small global annual mean value of -0.04±0.03 W m^{-2}. However, stronger positive effect can be found in the western Pacific (3.0 W m^{-2}) and Arctic regions (1.0 W m^{-2}). The global annual mean CRE of

Atmos. Chem. Phys. Discuss., doi:10.5194/acp-2016-167, 2016
Manuscript under review for journal Atmos. Chem. Phys.
Published: 1 April 2016

fire POM is -0.59±0.03 W m^{-2} (Figure 8c), and dominates the cloud effect of all fire aerosols. The sum of CRE from fire BC and POM (-0.62±0.03 W m^{-2}) is smaller than that of all fire aerosols (-0.70±0.05 W m^{-2}) due to the non-linear interactions of fire BC and fire POM as well as the negative CRE of fire sulfate.

The seasonal variation of all fire aerosol CRE is shown in Figure 9. The maximum of fire aerosol CRE is in the boreal summer (i.e., the fire season in NH) located in the NH high latitudes (60°N to 90°N). The largest summer CRE is found in the land areas and is as large as -15 W m^{-2}. The fire aerosol CRE in the tropical regions is most significant in the boreal summer (up to -15 W m^{-2}) and autumn (up to -10 W m^{-2}) over the ocean areas. The different spatial distributions of fire aerosol CRE in the NH high latitudes and in the tropics result from the difference in cloud distributions between the two regions. During the fire season the cloud LWP over the land areas in the NH mid- and high latitudes is three times larger than that over the ocean areas in the tropics. Larger cloud LWP favors the stronger CRE. Like the fire aerosol DRE, the smallest fire aerosol CRE occurs in the boreal spring.

Seasonal variations of zonal mean fire aerosol DRE, CRE, cloud LWP, low-level cloud amount, and vertically-integrated (burden) concentrations of fire POM and fire BC are shown in Figure 10. The seasonal variation of fire BC and fire POM burdens is largest in the SH low latitudes (from 30°S to 0°N) and NH mid- and high latitudes (50°N to 90°N). Distinct features of these two areas can also be noticed that the maximum fire BC burden in NH (0.3 mg m^{-2}) is much lower than that in SH (0.8 mg m^{-2}), while the maximum POM burdens in these two areas are comparable.

Interestingly, the DRE is larger in the NH summer than that in the SH autumn although the fire BC burden is much lower in the NH summer. It is mainly due to the larger amount of low clouds in the NH high latitudes, which enhances the absorption of fire BC. The maximum DRE in the NH summer is found near the North Pole (70 °N to 90 °N), and not around 60 °N where the fire aerosol burden is highest. The CRE of fire aerosols is about 3 times larger in the NH summer than that in the SH autumn, although the burden of fire POM in NH is comparable to that in SH. The larger cloud LWP in the NH summer around 40-60°N and higher fire OC/BC ratios favor the stronger CRE there.

3.4 Surface snow albedo effect

Here we compare the modeled BC-in-snow (BCS) concentrations with observation data collected from multiple field campaigns over the Arctic [*Doherty et al.*, 2010] and Northern China [*Wang et al.*, 2013; *Qian et al.*, 2014]. Figure 11a shows the simulated (from FIRE and NOFIRE experiments) and observed BCS concentrations as a function of latitude. The range of observed BCS concentrations is between 1 and 200 ng g^{-1} in the Arctic and between 50 and 2000 ng g^{-1} in Northern China, respectively. Both FIRE and NOFIRE experiments capture the meridional gradient in BCS concentrations between the mid-latitudes (Northern China) and high latitudes (Arctic). The mean and median concentrations of BCS are both overestimated in Northern China, implying the high biases from the anthropogenic emissions and/or model physics (Figure 11b). The mean and median BCS

Atmos. Chem. Phys. Discuss., doi:10.5194/acp-2016-167, 2016
Manuscript under review for journal Atmos. Chem. Phys.
Published: 1 April 2016

concentrations from the FIRE experiment agree better with observations than those from the NOFIRE experiment in the Arctic (Figure 11b). This suggests that fire emissions are important for BCS concentrations in the Arctic.

The annual mean SAE of all fire aerosols diagnosed from *Ghan* [2013] and the fire BCS effect diagnosed from SNICAR are shown in Figure 12. The global annual mean SAE (0.03±0.10 W m^{-2}) is much smaller compared to the DRE and CRE. The SAE over land is maximum in spring (0.12±0.27 W m^{-2}) and winter (0.06±0.16 W m^{-2}). The SAE over land in summer and autumn is very small (less than 0.01 W m^{-2}). We note that the mean SAE calculated with *Ghan* [2013] is much smaller than the standard deviation resulted from the internal variability.

The annual mean fire BCS effect calculated from SNICAR is shown in Figure 12b and 12c. The spatial distribution of the fire BCS effect is similar to the fire SAE, implying that the fire SAE has a significant contribution from the fire BCS effect. Averaged when only snow is present, the fire BCS effect is larger (0.048 W m^{-2}). The global mean fire BCS effect (with the presence of snow) can be as large as 0.06 W m^{-2} in spring, and the maximum effect (up to 1 W m^{-2}) is located in the Arctic regions (East Siberia, Alaska and Greenland, figure not shown). The positive SAE in Siberia, North America and Canada can be a result of BCS effect. However, the SAE in these regions is larger than the BCS forcing especially in spring. The snow melting and snow depth change due to the BCS warming may induce a larger positive SAE than the albedo change due to BCS itself. The negative SAE over land is a result of the snow depth change caused by fire aerosols.

Atmos. Chem. Phys. Discuss., doi:10.5194/acp-2016-167, 2016
Manuscript under review for journal Atmos. Chem. Phys.
Published: 1 April 2016

3.5 Fire aerosol effects on shortwave radiation, global temperature and precipitation

Here, we show the annual mean net shortwave flux change at TOA (i.e., total radiative effect), in the atmosphere and at surface, and changes in surface air temperature, convective and large-scale precipitation due to all fire aerosols in Figure 13 and Table 2. The global mean net shortwave flux change at TOA due to all fire aerosols is -0.55±0.07 W m^{-2}, which indicates that fire aerosols lead to the reduction of shortwave flux into the Earth's system. The zonal mean TOA shortwave flux reduction in the Arctic regions (-1.35±1.03 W m^{-2}) is much larger than that in the tropical regions (-0.66±0.09 W m^{-2}). The cooling at TOA is mostly from fire aerosol CRE. The maximum negative RE is located in the land areas of the Arctic and ocean areas of the tropics. Although the global mean total radiative effect is negative, positive effect is found in some land areas (e.g., Africa, Greenland).

The shortwave flux change in the atmosphere of the tropical regions is much larger than that of the Arctic regions. It is because BC burden in the tropics (0.17 mg m^{-2}) is larger than that in the Arctic (0.09 mg m^{-2}). Strong absorption (~8 W m^{-2}) in the atmosphere is found in the land areas of South Africa and South America and in the Southeast Atlantic. The surface shortwave flux change in the Arctic is mostly from the TOA shortwave flux reduction due to the fire aerosol CRE, while the surface shortwave flux change in the tropics is mostly due to the fire BC absorption in the atmosphere.

The fire aerosols lead to the reduction of the global mean surface air temperature

(T_s) by 0.03±0.03 K, consistent with the reduction of shortwave fluxes at TOA and at surface. The largest surface cooling is found in the Arctic and tropical regions by up to 0.6 K. The cooling of the Arctic is related to the strong fire aerosol CRE, while the cooling in the tropics is mainly from the surface shortwave flux reduction due to the fire BC absorption. The T_s change in the ocean areas is very small since the SST is prescribed in our simulations.

The global mean total precipitation is reduced by 0.010±0.002 mm day^{-1} due to all fire aerosols (Table 2). Unlike the T_s change, the precipitation reduction in the tropics (0.016 mm day^{-1}) is much larger than that in the Arctic (0.001 mm day^{-1}). The reduction in the tropics is mainly from the large-scale precipitation decrease (0.015 mm day^{-1}). The net change in the convective precipitation is very small in the tropics (0.001 mm day^{-1}), as the convective precipitation is significantly decreased near the equator and increased in the regions away from the equator, consistent with the results of *Tosca et al.* [2013]. The shortwave flux reduction at surface leads to a stabilization of the atmospheric boundary layer and a suppression of the convection near the equator. The strong atmospheric absorption by fire BC leads to the reduction of low-level clouds and large-scale precipitation in the tropics. Both effects lead to a significant reduction of total precipitation near the equator. The precipitation decrease in the NH high latitudes is mainly from the reduction of convective precipitation.

Figure 14 shows the changes of T_s, total precipitation, cloud LWP, and low-level cloud cover in the summer due to all fire aerosols. The T_s is reduced by more than 1 K in most of land areas around 60°N. The maximum cooling (larger than 1.5 K) is found

in East Siberia, Alaska and Canada. A decrease of total precipitation (by about 0.2 mm day^{-1}) is found in these regions. Accompanying the surface cooling and precipitation reduction, a significant increase of cloud LWP and low-level cloud cover is found there. This is a result of the indirect effect of fire aerosols in the land areas of the Arctic (60°N to 90°N). The fire POM leads to the reduction of cloud droplet effect radius and the increase of cloud droplet number concentration, consistent with observed fire effects on clouds in Canada and the United States [*Peng et al.*, 2002].

4. Discussion and Conclusions

In our study, the fire aerosol radiative effect (RE) is calculated with CESM. The method from *Ghan* [2013] is used to diagnose the DRE, CRE and SAE of fire aerosols. Additional experiment with CESM which tracks the wildfire BC and POM separately from fossil fuel and biofuel sources is performed to diagnose the fire aerosol DRE and fire BC-in-snow effect for comparisons with the *Ghan* [2013] method.

The BC and POM burdens from wildfires are largest in the tropical regions (South Africa, South America and Southeast Asia) and in the NH mid- to high latitudes (North of 45°N) (Northeast Asia, Alaska and Canada). Fire aerosols contribute 41% and 70% to the global burden of BC and POM, respectively. When comparing with the AERONET AOD and SSA data, modeled monthly AOD agrees with observations within a factor of 2 for most of the South African and South American sites. The model underestimation of AOD is found in the South American

sites near fire source regions, which is most obvious in the fire season (September and October). The model underestimates the observed AOD in the Arctic regions in both fire and non-fire seasons. The modeled SSA in South Africa and South America is generally in agreement with observations, while the modeled SSA in the Arctic is lower.

The annual mean DRE of all fire aerosols is 0.155±0.01 W m^{-2} and positive over most areas except in some land areas (e.g., South Africa, North Canada, and East Siberia). The annual maximum DRE is found in the oceanic areas west of South Africa (5 W m^{-2}) and South America (1.5 W m^{-2}). The positive DRE over the land regions of South Africa and South America is smaller, although the fire aerosol burdens are higher. It is because the larger amount of low-level clouds in the oceanic areas reflects the solar radiation back to the space for more absorption by fire BC above clouds, and thus generates a larger positive DRE at TOA. The annual mean DRE of fire BC is about 0.25±0.01 W m^{-2} and positive over the globe. Fire POM induces a weak negative DRE globally (-0.05 W m^{-2}) with the BBFFBF method and a small positive value (0.04±0.01 W m^{-2}) with the *Ghan* [2013] method. The positive DRE of fire POM is found over oceanic areas west of South Africa and South America, North Pacific, and polar regions where the low-level cloud coverage is large or the surface albedo is higher. The maximum DRE in the Arctic regions occurs in the summer (0.35 W m^{-2}), while the DRE in the tropical regions reaches its maximum in the autumn.

The global annual mean CRE of all fire aerosols is -0.70±0.05 W m^{-2} and the

Atmos. Chem. Phys. Discuss., doi:10.5194/acp-2016-167, 2016
Manuscript under review for journal Atmos. Chem. Phys.
Published: 1 April 2016

maximum forcing is located in the ocean areas west of South Africa and South America and land areas of the NH high latitudes. The maximum fire aerosol CRE occurs in the NH high latitudes in the boreal summer, which results from the large cloud LWP over the land areas and the large fire OC to BC ratio. Associated with the strong indirect effects of fire aerosols in the Arctic summer, significant surface cooling, precipitation reduction, and low-level cloud cover increase are found in these regions.

Modeled BCS concentrations from the FIRE experiment are evaluated against observations in Northern China and in the Arctic, and generally agree with the observations for the mean and median values in the Arctic regions. The high bias of modeled BCS concentrations in Northern China may not result from the fire BC because differences in BCS concentrations between FIRE and NOFIRE experiments are very small in North China. The global annual mean SAE is 0.03±0.10 W m^{-2} with the maximum effect in spring (0.12 W m^{-2}). The SAE is mainly due to the effect of fire BC deposit on snow (0.02 W m^{-2}) diagnosed from SNICAR with the maximum effect as large as 0.06 W m^{-2} (when snow is present) in spring.

The fire aerosols reduce the global mean surface air temperature (T_s) by 0.03± 0.03 K and precipitation by 0.01±0.002 mm day^{-1}. The maximum cooling (~1 K) due to fire aerosols occurs around 60°N in summer, and a suppression of precipitation (~0.1 mm day^{-1}) is also found there. The strong cooling is a result of the strong indirect effects (-15 W m^{-2}) in the land areas of the Arctic regions (60°N to 90°N).

In our study, the global radiative effect of fire aerosols is estimated from

Atmos. Chem. Phys. Discuss., doi:10.5194/acp-2016-167, 2016
Manuscript under review for journal Atmos. Chem. Phys.
Published: 1 April 2016

simulations performed with the 4-mode version Modal aerosol module (MAM4) [*Liu et al.*, 2016], daily fire emissions with prescribed vertical emission profiles, and higher model resolution (0.9° by 1.25°) compared to earlier modeling studies of fire aerosols [*Tosca et al.*, 2013; *Ward et al.*, 2012]. In their studies, the GFED fire aerosol emissions were increased by a factor of 1-3 depending on regions to match the observed AOD. In our study, we do not apply the scaling factor to the fire aerosol emissions. Our global annual mean DRE of fire aerosols (0.155±0.01 W m^{-2}) is, however, close to 0.18 W m^{-2} in *Tosca et al.* [2013] and 0.13 W m^{-2} in *Ward et al.* [2012]. The similar fire aerosol DRE from our study but with smaller fire emissions than these previous studies can result from (1) the use of MAM4 in our study which more realistically represents the external/internal mixing of BC with other soluble aerosol species; (2) the more accurate estimation of DRE of fire aerosols in the presence of low-level clouds with the method of *Ghan* [2013]; and (3) the inclusion of vertical emissions of fire aerosols, which allows more efficient transport of fire aerosols from sources. The CRE due to fire aerosols in our study (-0.70±0.05 W m^{-2}) is smaller than -1.64 W m^{-2} in *Ward et al.* [2012] due to the lower fire POM emissions used in this study compared to *Ward et al.* [2012]. We note that the model still underestimates observed AODs (mostly within a factor of 2) at the sites predominantly influenced by biomass burning aerosols during the fire season, which implies that the fire aerosol radiative forcing can be stronger than estimated in this study.

Acknowledgments

This work is supported by the Office of Science of the US Department of Energy (DOE) as the NSF-DOE-USDA Joint Earth System Modeling (EaSM) Program and the National Natural Science Foundation of China (NSFC) under Grant No.41505062. The Pacific Northwest National Laboratory is operated for the DOE by the Battelle Memorial Institute under contract DE-AC05-76RL01830. The authors would like to acknowledge the use of computational resources (ark:/85065/d7wd3xhc) at the NCAR-Wyoming Supercomputing Center provided by the National Science Foundation and the State of Wyoming, and supported by NCAR's Computational and Information Systems Laboratory. The fire emission data were obtained from the Global Fire Emissions Database (GFED, http://www.globalfiredata.org). The AERONET data were obtained from http://aeronet.gsfc.nasa.gov. We thank Xiangjun Shi for the help with processing the AERONET data.

References

Abel, S. J., Highwood, E. J., Haywood, J. M., and Stringer, M. A.: The direct radiative effect of biomass burning aerosols over southern Africa, Atmos. Chem. Phys., 5, 1999-2018, 10.5194/acp-5-1999-2005, 2005.

Ackerman, A. S., Toon, O. B., Stevens, D. E., Heymsfield, A. J., Ramanathan, V., and Welton, E. J.: Reduction of Tropical Cloudiness by Soot, Science, 288, 1042-1047, 10.1126/science.288.5468.1042, 2000.

Andreae, M. O., and Rosenfeld, D.: Aerosol–cloud–precipitation interactions. Part 1. The nature and sources of cloud-active aerosols, Earth-Science Reviews, 89, 13-41, http://dx.doi.org/10.1016/j.earscirev.2008.03.001, 2008.

Andreae, M. O., Rosenfeld, D., Artaxo, P., Costa, A. A., Frank, G. P., Longo, K. M., and Silva-Dias, M. A. F.: Smoking Rain Clouds over the Amazon, Science, 303, 1337-1342, 10.1126/science.1092779, 2004.

Bond, T. C., Doherty, S. J., Fahey, D. W., Forster, P. M., Berntsen, T., DeAngelo, B. J., Flanner, M. G., Ghan, S., Karcher, B., Koch, D., Kinne, S., Kondo, Y., Quinn, P. K., Sarofim, M. C., Schultz, M. G., Schulz, M., Venkataraman, C., Zhang, H., Zhang, S., Bellouin, N., Guttikunda, S. K., Hopke, P. K., Jacobson, M. Z., Kaiser, J. W., Klimont, Z., Lohmann, U., Schwarz, J. P., Shindell, D., Storelvmo, T., Warren, S. G., and Zender, C. S.: Bounding the role of black carbon in the climate system: A scientific assessment, J Geophys Res-Atmos, 118, 5380-5552, Doi 10.1002/Jgrd.50171, 2013.

Boucher, O., and Tanré, D.: Estimation of the aerosol perturbation to the Earth's Radiative Budget over oceans using POLDER satellite aerosol retrievals, Geophysical Research Letters, 27, 1103-1106, 10.1029/1999GL010963, 2000.

Bowman, D. M. J. S., Balch, J. K., Artaxo, P., Bond, W. J., Carlson, J. M., Cochrane, M. A., D'Antonio, C. M., DeFries, R. S., Doyle, J. C., Harrison, S. P., Johnston, F. H., Keeley, J. E., Krawchuk, M. A., Kull, C. A., Marston, J. B., Moritz, M. A., Prentice, I. C., Roos, C. I., Scott, A. C., Swetnam, T. W., van der Werf, G. R., and Pyne, S. J.: Fire in the Earth System, Science, 324, 481-484, 10.1126/science.1163886, 2009.

Carslaw, K. S., Boucher, O., Spracklen, D. V., Mann, G. W., Rae, J. G. L., Woodward, S., and Kulmala, M.: A review of natural aerosol interactions and feedbacks within the Earth system, Atmos. Chem. Phys., 10, 1701-1737, 10.5194/acp-10-1701-2010, 2010.

Chuang, C. C., Penner, J. E., Prospero, J. M., Grant, K. E., Rau, G. H., and Kawamoto, K.: Cloud susceptibility and the first aerosol indirect forcing: Sensitivity to black carbon and aerosol concentrations, Journal of Geophysical Research: Atmospheres, 107, 4564, 10.1029/2000JD000215, 2002.

Ciais, P., Sabine, C., Bala, G., Bopp, L., Brovkin, V., Canadell, J., Chhabra, A., DeFries, R., Galloway, J., Heimann, M., Jones, C., Le Quéré, C., Myneni, R. B., Piao, S., and Thornton, P.: Carbon and Other Biogeochemical Cycles, in: Climate Change 2013: The Physical Science Basis. Contribution of Working Group I to the Fifth Assessment Report of the Intergovernmental Panel on Climate Change,

edited by: Stocker, T. F., Qin, D., Plattner, G.-K., Tignor, M., Allen, S. K., Boschung, J., Nauels, A., Xia, Y., Bex, V., and Midgley, P. M., Cambridge University Press, Cambridge, United Kingdom and New York, NY, USA, 465–570, 2013.

Cohen, J. B., and Wang, C.: Estimating global black carbon emissions using a top-down Kalman Filter approach, Journal of Geophysical Research: Atmospheres, 119, 2013JD019912, 10.1002/2013JD019912, 2014.

Dentener, F., Kinne, S., Bond, T., Boucher, O., Cofala, J., Generoso, S., Ginoux, P., Gong, S., Hoelzemann, J. J., Ito, A., Marelli, L., Penner, J. E., Putaud, J. P., Textor, C., Schulz, M., van der Werf, G. R., and Wilson, J.: Emissions of primary aerosol and precursor gases in the years 2000 and 1750 prescribed data-sets for AeroCom, Atmos. Chem. Phys., 6, 4321-4344, 10.5194/acp-6-4321-2006, 2006.

Doherty, S. J., Warren, S. G., Grenfell, T. C., Clarke, A. D., and Brandt, R. E.: Light-absorbing impurities in Arctic snow, Atmos. Chem. Phys., 10, 11647-11680, 10.5194/acp-10-11647-2010, 2010.

Flanner, M. G., and Zender, C. S.: Snowpack radiative heating: Influence on Tibetan Plateau climate, Geophysical Research Letters, 32, L06501, Artn L06501, Doi 10.1029/2004gl022076, 2005.

Flanner, M. G., Zender, C. S., Randerson, J. T., and Rasch, P. J.: Present-day climate forcing and response from black carbon in snow, Journal of Geophysical Research: Atmospheres, 112, D11202, 10.1029/2006JD008003, 2007.

Flanner, M. G., Zender, C. S., Hess, P. G., Mahowald, N. M., Painter, T. H., Ramanathan, V., and Rasch, P. J.: Springtime warming and reduced snow cover from carbonaceous particles, Atmos. Chem. Phys., 9, 2481-2497, 10.5194/acp-9-2481-2009, 2009.

Forster, P., Ramaswamy, V., Artaxo, P., Berntsen, T., Betts, R., Fahey, D. W., Haywood, J., Lean, J., Lowe, D. C., and Myhre, G.: Changes in atmospheric constituents and in radiative forcing. Chapter 2, in: Climate Change 2007. The Physical Science Basis, 2007.

Ghan, S. J.: Technical Note: Estimating aerosol effects on cloud radiative forcing,

Atmos. Chem. Phys., 13, 9971-9974, 10.5194/acp-13-9971-2013, 2013.

Giglio, L., Randerson, J. T., and van der Werf, G. R.: Analysis of daily, monthly, and annual burned area using the fourth-generation global fire emissions database (GFED4), Journal of Geophysical Research: Biogeosciences, 118, 317-328, 10.1002/jgrg.20042, 2013.

Hansen, J., Sato, M., Ruedy, R., Nazarenko, L., Lacis, A., Schmidt, G. A., Russell, G., Aleinov, I., Bauer, M., Bauer, S., Bell, N., Cairns, B., Canuto, V., Chandler, M., Cheng, Y., Del Genio, A., Faluvegi, G., Fleming, E., Friend, A., Hall, T., Jackman, C., Kelley, M., Kiang, N., Koch, D., Lean, J., Lerner, J., Lo, K., Menon, S., Miller, R., Minnis, P., Novakov, T., Oinas, V., Perlwitz, J., Perlwitz, J., Rind, D., Romanou, A., Shindell, D., Stone, P., Sun, S., Tausnev, N., Thresher, D., Wielicki, B., Wong, T., Yao, M., and Zhang, S.: Efficacy of climate forcings, Journal of Geophysical Research: Atmospheres, 110, D18104, 10.1029/2005JD005776, 2005.

Heald, C. L., Ridley, D. A., Kroll, J. H., Barrett, S. R. H., Cady-Pereira, K. E., Alvarado, M. J., and Holmes, C. D.: Contrasting the direct radiative effect and direct radiative forcing of aerosols, Atmos. Chem. Phys., 14, 5513-5527, 10.5194/acp-14-5513-2014, 2014.

Houghton, J. T.: Climate change 1995: The science of climate change: contribution of working group I to the second assessment report of the Intergovernmental Panel on Climate Change, Cambridge University Press, 1996.

IPCC (2013), Climate Change 2013: The Physical Science Basis. Contribution of Working Group I to the Fifth Assessment Report of the Intergovernmental Panel on Climate Change, 1535 pp., Cambridge University Press, Cambridge, United Kingdom and New York, NY, USA, doi:10.1017/CBO9781107415324.

Jacobson, M. Z.: Climate response of fossil fuel and biofuel soot, accounting for soot's feedback to snow and sea ice albedo and emissivity, Journal of Geophysical Research: Atmospheres, 109, D21201, 10.1029/2004JD004945, 2004.

Jones, A., Haywood, J. M., and Boucher, O.: Aerosol forcing, climate response and climate sensitivity in the Hadley Centre climate model, Journal of Geophysical

Research: Atmospheres, 112, D20211, 10.1029/2007JD008688, 2007.

Kaiser, J. W., Heil, A., Andreae, M. O., Benedetti, A., Chubarova, N., Jones, L., Morcrette, J. J., Razinger, M., Schultz, M. G., Suttie, M., and van der Werf, G. R.: Biomass burning emissions estimated with a global fire assimilation system based on observed fire radiative power, Biogeosciences, 9, 527-554, 10.5194/bg-9-527-2012, 2012.

Keywood, M., Kanakidou, M., Stohl, A., Dentener, F., Grassi, G., Meyer, C. P., Torseth, K., Edwards, D., Thompson, A. M., Lohmann, U., and Burrows, J.: Fire in the Air: Biomass Burning Impacts in a Changing Climate, Critical Reviews in Environmental Science and Technology, 43, 40-83, 10.1080/10643389.2011.604248, 2011.

Koch, D., Menon, S., Del Genio, A., Ruedy, R., Alienov, I., and Schmidt, G. A.: Distinguishing Aerosol Impacts on Climate over the Past Century, Journal of Climate, 22, 2659-2677, 10.1175/2008JCLI2573.1, 2009.

Koch, D., Balkanski, Y., Bauer, S. E., Easter, R. C., Ferrachat, S., Ghan, S. J., Hoose, C., Iversen, T., Kirkevåg, A., Kristjansson, J. E., Liu, X., Lohmann, U., Menon, S., Quaas, J., Schulz, M., Seland, Ø., Takemura, T., and Yan, N.: Soot microphysical effects on liquid clouds, a multi-model investigation, Atmos. Chem. Phys., 11, 1051-1064, 10.5194/acp-11-1051-2011, 2011.

Koch, D., and Del Genio, A. D.: Black carbon semi-direct effects on cloud cover: review and synthesis, Atmos. Chem. Phys., 10, 7685-7696, 10.5194/acp-10-7685-2010, 2010.

Koren, I., Kaufman, Y. J., Rosenfeld, D., Remer, L. A., and Rudich, Y.: Aerosol invigoration and restructuring of Atlantic convective clouds, Geophysical Research Letters, 32, L14828, 10.1029/2005GL023187, 2005.

Lamarque, J. F., Bond, T. C., Eyring, V., Granier, C., Heil, A., Klimont, Z., Lee, D., Liousse, C., Mieville, A., Owen, B., Schultz, M. G., Shindell, D., Smith, S. J., Stehfest, E., Van Aardenne, J., Cooper, O. R., Kainuma, M., Mahowald, N., McConnell, J. R., Naik, V., Riahi, K., and van Vuuren, D. P.: Historical (1850–2000) gridded anthropogenic and biomass burning emissions of reactive gases and

aerosols: methodology and application, Atmos. Chem. Phys., 10, 7017-7039, 10.5194/acp-10-7017-2010, 2010.

Liu, X., J. E. Penner, B. Das, D. Bergmann, J. M. Rodriguez, S. Strahan, M. Wang and Y. Feng: Uncertainties in global aerosol simulations: Assessment using three meteorological datasets, Journal of Geophysical Research, 112, D11212, doi:10.1029/2006JD008216, 2007.

Liu, X., Easter, R. C., Ghan, S. J., Zaveri, R., Rasch, P., Shi, X., Lamarque, J. F., Gettelman, A., Morrison, H., Vitt, F., Conley, A., Park, S., Neale, R., Hannay, C., Ekman, A. M. L., Hess, P., Mahowald, N., Collins, W., Iacono, M. J., Bretherton, C. S., Flanner, M. G., and Mitchell, D.: Toward a minimal representation of aerosols in climate models: description and evaluation in the Community Atmosphere Model CAM5, Geosci. Model Dev., 5, 709-739, 10.5194/gmd-5-709-2012, 2012.

Liu, X., Ma, P. L., Wang, H., Tilmes, S., Singh, B., Easter, R. C., Ghan, S. J., and Rasch, P. J.: Description and evaluation of a new four-mode version of the Modal Aerosol Module (MAM4) within version 5.3 of the Community Atmosphere Model, Geosci. Model Dev., 9, 505-522, 10.5194/gmd-9-505-2016, 2016.

Liu, Y.: Atmospheric response and feedback to radiative forcing from biomass burning in tropical South America, Agricultural and Forest Meteorology, 133, 40-53, http://dx.doi.org/10.1016/j.agrformet.2005.03.011, 2005.

Liu, Y., Goodrick, S., and Heilman, W.: Wildland fire emissions, carbon, and climate: Wildfire–climate interactions, Forest Ecology and Management, 317, 80-96, http://dx.doi.org/10.1016/j.foreco.2013.02.020, 2014.

Lu, Z., and Sokolik, I. N.: The effect of smoke emission amount on changes in cloud properties and precipitation: A case study of Canadian boreal wildfires of 2007, Journal of Geophysical Research: Atmospheres, 118, 2013JD019860, 10.1002/2013JD019860, 2013.

Ma, P. L., Rasch, P. J., Fast, J. D., Easter, R. C., Gustafson Jr, W. I., Liu, X., Ghan, S. J., and Singh, B.: Assessing the CAM5 physics suite in the WRF-Chem model: implementation, resolution sensitivity, and a first evaluation for a regional case

study, Geosci. Model Dev., 7, 755-778, 10.5194/gmd-7-755-2014, 2014.

Marlon, J. R., Bartlein, P. J., Walsh, M. K., Harrison, S. P., Brown, K. J., Edwards, M. E., Higuera, P. E., Power, M. J., Anderson, R. S., Briles, C., Brunelle, A., Carcaillet, C., Daniels, M., Hu, F. S., Lavoie, M., Long, C., Minckley, T., Richard, P. J. H., Scott, A. C., Shafer, D. S., Tinner, W., Umbanhowar, C. E., and Whitlock, C.: Wildfire responses to abrupt climate change in North America, Proceedings of the National Academy of Sciences, 106, 2519-2524, 10.1073/pnas.0808212106, 2009.

McCarthy, J. J.: Climate change 2001: impacts, adaptation, and vulnerability: contribution of Working Group II to the third assessment report of the Intergovernmental Panel on Climate Change, Cambridge University Press, 2001.

Morrison, H., and Gettelman, A.: A New Two-Moment Bulk Stratiform Cloud Microphysics Scheme in the Community Atmosphere Model, Version 3 (CAM3). Part I: Description and Numerical Tests, Journal of Climate, 21, 3642-3659, doi:10.1175/2008JCLI2105.1, 2008.

Myhre, G., Samset, B. H., Schulz, M., Balkanski, Y., Bauer, S., Berntsen, T. K., Bian, H., Bellouin, N., Chin, M., Diehl, T., Easter, R. C., Feichter, J., Ghan, S. J., Hauglustaine, D., Iversen, T., Kinne, S., Kirkevåg, A., Lamarque, J. F., Lin, G., Liu, X., Lund, M. T., Luo, G., Ma, X., van Noije, T., Penner, J. E., Rasch, P. J., Ruiz, A., Seland, Ø., Skeie, R. B., Stier, P., Takemura, T., Tsigaridis, K., Wang, P., Wang, Z., Xu, L., Yu, H., Yu, F., Yoon, J. H., Zhang, K., Zhang, H., and Zhou, C.: Radiative forcing of the direct aerosol effect from AeroCom Phase II simulations, Atmos. Chem. Phys., 13, 1853-1877, 10.5194/acp-13-1853-2013, 2013.

Myhre, G., Shindell, D., Bréon, F.-M., Collins, W., Fuglestvedt, J., Huang, J., Koch, D., Lamarque, J.-F., Lee, D., Mendoza, B., Nakajima, T., Robock, A., Stephens, G., Takemura, T., and Zhang, H.: Anthropogenic and Natural Radiative Forcing, in: Climate Change 2013: The Physical Science Basis. Contribution of Working Group I to the Fifth Assessment Report of the Intergovernmental Panel on Climate Change, edited by: Stocker, T. F., Qin, D., Plattner, G.-K., Tignor, M., Allen, S.

K., Boschung, J., Nauels, A., Xia, Y., Bex, V., and Midgley, P. M., Cambridge University Press, Cambridge, United Kingdom and New York, NY, USA, 659–740, 2013.

Neale, R., Chen, C., Gettelman, A., Lauritzen, P., Park, S., Williamson, D., Garcia, R., Kinnison, D., Lamarque, J., and Marsh, D.: Description of the NCAR Community Atmosphere Model (CAM 5.0), 2010.

Oleson, K. W., Lawrence, D. M., Gordon, B., Flanner, M. G., Kluzek, E., Peter, J., Levis, S., Swenson, S. C., Thornton, E., and Feddema, J.: Technical description of version 4.0 of the Community Land Model (CLM), 2010.

Peng, Y., Lohmann, U., Leaitch, R., Banic, C., and Couture, M.: The cloud albedo-cloud droplet effective radius relationship for clean and polluted clouds from RACE and FIRE.ACE, Journal of Geophysical Research: Atmospheres, 107, AAC 1-1-AAC 1-6, 10.1029/2000JD000281, 2002.

Qian, Y., Flanner, M. G., Leung, L. R., and Wang, W.: Sensitivity studies on the impacts of Tibetan Plateau snowpack pollution on the Asian hydrological cycle and monsoon climate, Atmos. Chem. Phys., 11, 1929-1948, 10.5194/acp-11-1929-2011, 2011.

Qian, Y., Gong, D., Fan, J., Leung, L. R., Bennartz, R., Chen, D., and Wang, W.: Heavy pollution suppresses light rain in China: Observations and modeling, Journal of Geophysical Research: Atmospheres, 114, D00K02, 10.1029/2008JD011575, 2009.

Qian, Y., Wang, H., Zhang, R., Flanner, M. G., and Rasch, P. J.: A sensitivity study on modeling black carbon in snow and its radiative forcing over the Arctic and Northern China, Environmental Research Letters, 9, 064001, 10.1088/1748-9326/9/6/064001, 2014.

Qian, Y., Yasunari, T. J., Doherty, S. J., Flanner, M. G., Lau, W. K. M., Ming, J., Wang, H., Wang, M., Warren, S. G., and Zhang, R.: Light-absorbing particles in snow and ice: Measurement and modeling of climatic and hydrological impact, Advances in Atmospheric Sciences, 32, 64-91, 10.1007/s00376-014-0010-0, 2014.

Quinn, P. K., Bates, T. S., Baum, E., Doubleday, N., Fiore, A. M., Flanner, M., Fridlind, A., Garrett, T. J., Koch, D., Menon, S., Shindell, D., Stohl, A., and Warren, S. G.: Short-lived pollutants in the Arctic: their climate impact and possible mitigation strategies, Atmos. Chem. Phys., 8, 1723-1735, 10.5194/acp-8-1723-2008, 2008.

Randerson, J. T., Liu, H., Flanner, M. G., Chambers, S. D., Jin, Y., Hess, P. G., Pfister, G., Mack, M. C., Treseder, K. K., Welp, L. R., Chapin, F. S., Harden, J. W., Goulden, M. L., Lyons, E., Neff, J. C., Schuur, E. A. G., and Zender, C. S.: The Impact of Boreal Forest Fire on Climate Warming, Science, 314, 1130-1132, 2006.

Rypdal, K., Rive, N., Berntsen, T. K., Klimont, Z., Mideksa, T. K., Myhre, G., and Skeie, R. B.: Costs and global impacts of black carbon abatement strategies, Tellus B, 61, 625-641, 10.1111/j.1600-0889.2009.00430.x, 2009.

Skeie, R. B., Berntsen, T., Myhre, G., Pedersen, C. A., Ström, J., Gerland, S., and Ogren, J. A.: Black carbon in the atmosphere and snow, from pre-industrial times until present, Atmos. Chem. Phys., 11, 6809-6836, 10.5194/acp-11-6809-2011, 2011.

Sommers, W. T., Loehman, R. A., and Hardy, C. C.: Wildland fire emissions, carbon, and climate: Science overview and knowledge needs, Forest Ecology and Management, 317, 1-8, http://dx.doi.org/10.1016/j.foreco.2013.12.014, 2014.

Stohl, A., Klimont, Z., Eckhardt, S., Kupiainen, K., Shevchenko, V. P., Kopeikin, V. M., and Novigatsky, A. N.: Black carbon in the Arctic: the underestimated role of gas flaring and residential combustion emissions, Atmos. Chem. Phys., 13, 8833-8855, 10.5194/acp-13-8833-2013, 2013.

Tosca, M. G., Diner, D. J., Garay, M. J., and Kalashnikova, O. V.: Observational evidence of fire-driven reduction of cloud fraction in tropical Africa, Journal of Geophysical Research: Atmospheres, 2014JD021759, 10.1002/2014JD021759, 2014.

Tosca, M. G., Randerson, J. T., and Zender, C. S.: Global impact of smoke aerosols from landscape fires on climate and the Hadley circulation, Atmos. Chem. Phys.,

13, 5227-5241, 10.5194/acp-13-5227-2013, 2013.

van der Werf, G. R., Dempewolf, J., Trigg, S. N., Randerson, J. T., Kasibhatla, P. S., Giglio, L., Murdiyarso, D., Peters, W., Morton, D. C., Collatz, G. J., Dolman, A. J., and DeFries, R. S.: Climate regulation of fire emissions and deforestation in equatorial Asia, Proceedings of the National Academy of Sciences, 105, 20350-20355, 10.1073/pnas.0803375105, 2008.

van der Werf, G. R., Randerson, J. T., Giglio, L., Collatz, G. J., Mu, M., Kasibhatla, P. S., Morton, D. C., DeFries, R. S., Jin, Y., and van Leeuwen, T. T.: Global fire emissions and the contribution of deforestation, savanna, forest, agricultural, and peat fires (1997–2009), Atmos. Chem. Phys., 10, 11707-11735, 10.5194/acp-10-11707-2010, 2010.

Wang, H., Easter, R. C., Rasch, P. J., Wang, M., Liu, X., Ghan, S. J., Qian, Y., Yoon, J. H., Ma, P. L., and Vinoj, V.: Sensitivity of remote aerosol distributions to representation of cloud–aerosol interactions in a global climate model, Geosci. Model Dev., 6, 765-782, 10.5194/gmd-6-765-2013, 2013.

Wang, X., Doherty, S. J., and Huang, J.: Black carbon and other light-absorbing impurities in snow across Northern China, Journal of Geophysical Research: Atmospheres, 118, 1471-1492, 10.1029/2012JD018291, 2013.

Ward, D. S., Kloster, S., Mahowald, N. M., Rogers, B. M., Randerson, J. T., and Hess, P. G.: The changing radiative forcing of fires: global model estimates for past, present and future, Atmos. Chem. Phys., 12, 10857-10886, 10.5194/acp-12-10857-2012, 2012.

Westerling, A. L., Hidalgo, H. G., Cayan, D. R., and Swetnam, T. W.: Warming and earlier spring increase western U.S. forest wildfire activity, Science, 313, 940-943, 10.1126/science.1128834, 2006.

Wiedinmyer, C., Akagi, S. K., Yokelson, R. J., Emmons, L. K., Al-Saadi, J. A., Orlando, J. J., and Soja, A. J.: The Fire INventory from NCAR (FINN): a high resolution global model to estimate the emissions from open burning, Geosci. Model Dev., 4, 625-641, 10.5194/gmd-4-625-2011, 2011.

Zhang, Y., Fu, R., Yu, H., Qian, Y., Dickinson, R., Silva Dias, M. A. F., da Silva Dias,

P. L., and Fernandes, K.: Impact of biomass burning aerosol on the monsoon circulation transition over Amazonia, Geophysical Research Letters, 36, L10814, 10.1029/2009GL037180, 2009.

Zhang, Z., Meyer, K., Platnick, S., Oreopoulos, L., Lee, D., and Yu, H.: A novel method for estimating shortwave direct radiative effect of above-cloud aerosols using CALIOP and MODIS data, Atmos. Meas. Tech., 7, 1777-1789, 10.5194/amt-7-1777-2014, 2014.

Atmos. Chem. Phys. Discuss., doi:10.5194/acp-2016-167, 2016
Manuscript under review for journal Atmos. Chem. Phys.
Published: 1 April 2016

Table 1. Numerical experiments and associated fire aerosol emissions in each experiment.

Experiment	Ensembles	Fire BC	Fire POM	Fire SO_2
FIRE	10	On	On	On
NOFIRE	10	Off	Off	Off
NOFIREBC	10	Off	On	On
NOFIREPOM	10	On	Off	On
FIRE_BBFFBF	1	On	On	On

Atmos. Chem. Phys. Discuss., doi:10.5194/acp-2016-167, 2016
Manuscript under review for journal Atmos. Chem. Phys.
Published: 1 April 2016

Atmospheric Chemistry and Physics Discussions

Table 2. Global, tropics (25°S to 25°N) and Arctic (60°N to 90°N) annual mean fire aerosol (POM and BC) burdens (mg m^{-2}), fire aerosol AOD, total fire aerosol radiative effect (RE) at TOA (W m^{-2}), direct radiative effect (DRE, W m^{-2}), cloud radiative effect (CRE, W m^{-2}), and surface albedo effect (SAE, W m^{-2}), and changes in shortwave and longwave cloud forcings (W m^{-2}), cloud liquid water path (LWP) (g m^{-2}), low-level cloud cover (%), net solar fluxes at surface and in the atmosphere (W m^{-2}), surface air temperature (K), and precipitation (total, convective, and large-scale) (mm day^{-1}) due to all fire aerosols. Standard deviations about the 10-ensemble means are included.

	Global	Tropics (25°S to 25°N)	Arctic (60°N to 90°N)
Fire POM burden	1.25±0.01	1.87±0.01	1.70±0.08
Fire BC burden	0.106±0.001	0.17±0.001	0.09±0.004
Fire aerosol optical depth	0.008±0.001	0.012±0.001	0.007±0.0004
Total radiative effect (RE)	-0.55±0.07	-0.66±0.09	-1.35±1.03
Direct radiative effect (DRE)	0.155±0.01	0.172±0.017	0.428±0.028
Cloud radiative effect (CRE)	-0.70±0.05	-0.82±0.09	-1.38±0.23
Surface albedo effect (over land)	0.03±0.10	-0.04±0.06	0.09±0.80
Shortwave cloud forcing	-0.43±0.05	-0.45±0.08	-1.18±0.22
Longwave cloud forcing	-0.26±0.04	-0.35±0.07	-0.04±0.17
Cloud liquid water path	1.62±0.01	1.95±0.13	2.59±0.25
Low-level cloud cover	0.012±0.06	-0.055±0.05	0.46±0.45
Net solar flux at surface	-1.38±0.05	-1.91±0.12	-2.27±1.04
Net solar flux in the atmosphere	0.83±0.03	1.25±0.04	0.92±0.05
Surface air temperature	-0.03±0.03	-0.024±0.011	-0.15±0.2
Total precipitation rate	-0.010±0.002	-0.016±0.01	-0.001±0.02
Convective precipitation rate	-0.003±0.002	-0.001±0.009	-0.005±0.003
Large-scale precipitation rate	-0.007±0.002	-0.015±0.003	0.004±0.019

Atmos. Chem. Phys. Discuss., doi:10.5194/acp-2016-167, 2016
Manuscript under review for journal Atmos. Chem. Phys.
Published: 1 April 2016

Atmospheric Chemistry and Physics
Discussions

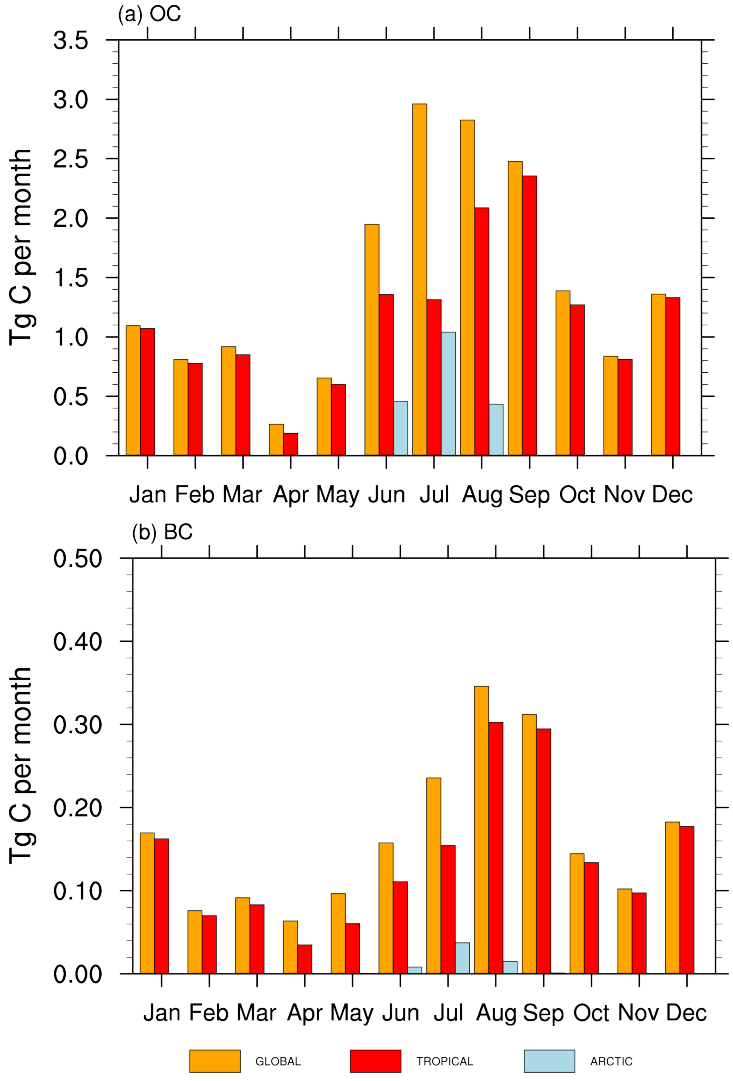

Figure 1. Seasonal variation of GFED monthly fire (a) organic carbon (OC) and (b) black carbon (BC) emissions (Tg C month^{-1}) averaged for the period of year 2003 to 2011 in the global, tropical (25°S to 25°N) and Arctic (60°N to 90°N) regions.

Atmos. Chem. Phys. Discuss., doi:10.5194/acp-2016-167, 2016
Manuscript under review for journal Atmos. Chem. Phys.
Published: 1 April 2016

Atmospheric Chemistry and Physics
Discussions

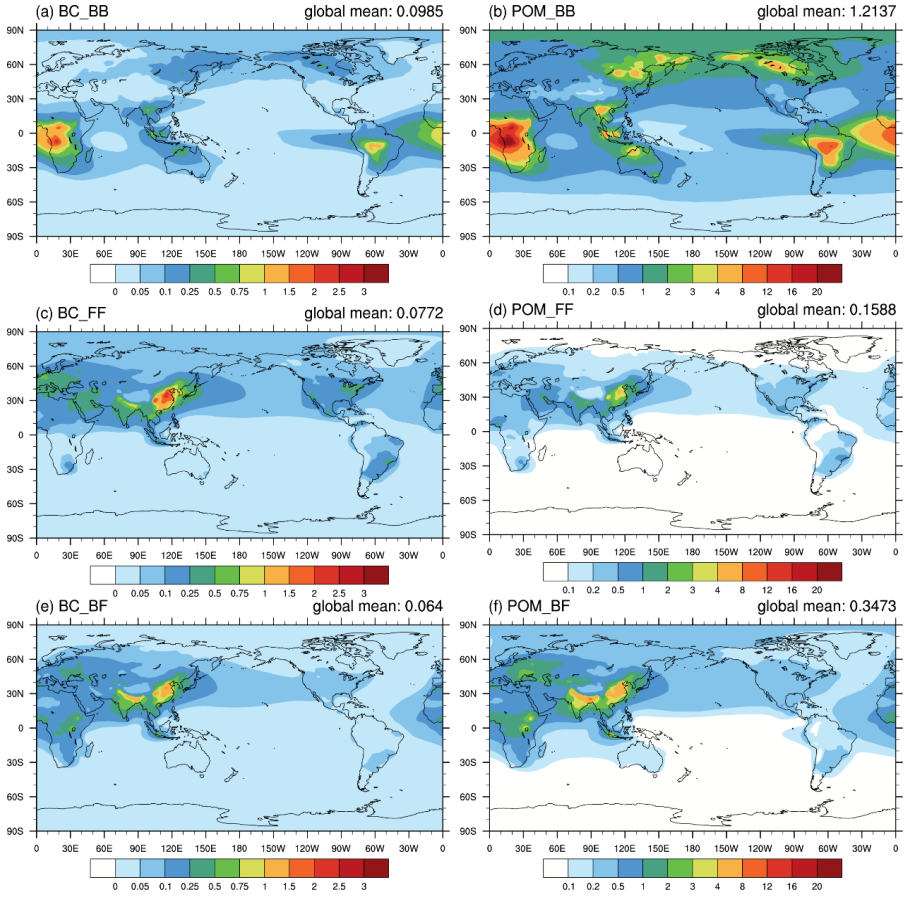

Figure 2. Annual mean (for year 2003-2011) vertically integrated concentrations (units: mg m^{-2}) of BC (left) and POM (right) from biomass burning (BB) (upper panel), FF (fossil fuel) (middle panel), and biofuel (BF) (lower panel).

Atmos. Chem. Phys. Discuss., doi:10.5194/acp-2016-167, 2016
Manuscript under review for journal Atmos. Chem. Phys.
Published: 1 April 2016

Atmospheric Chemistry and Physics
Discussions

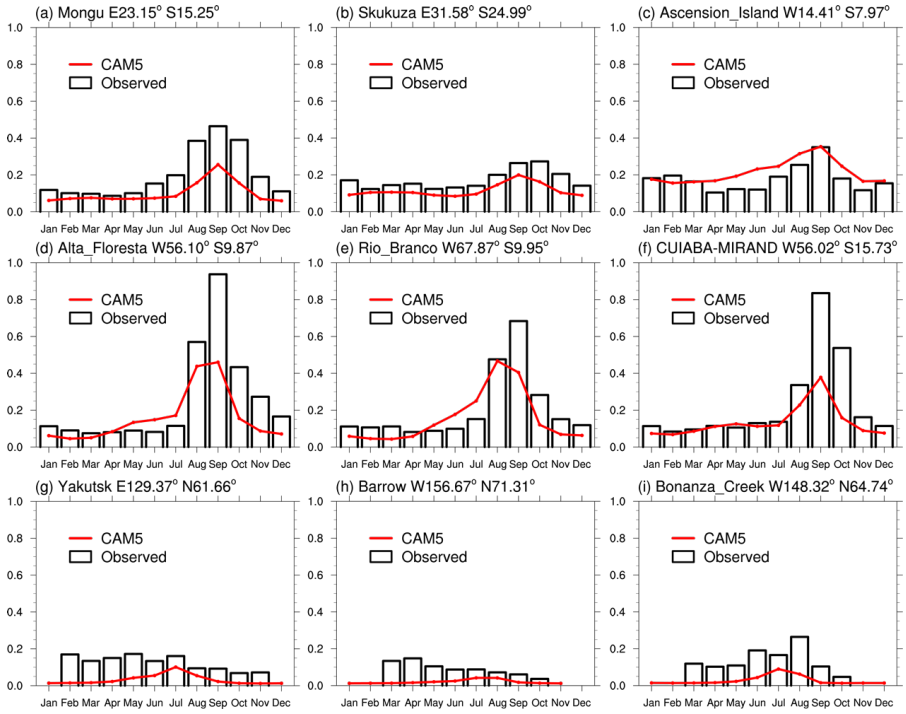

Figure 3. Comparison of modeled seasonal variations of aerosol optical depth (AOD) for the period of 2003-2011 with observations for the same period from the AERONET sites.

Atmos. Chem. Phys. Discuss., doi:10.5194/acp-2016-167, 2016
Manuscript under review for journal Atmos. Chem. Phys.
Published: 1 April 2016

Atmospheric Chemistry and Physics
Discussions

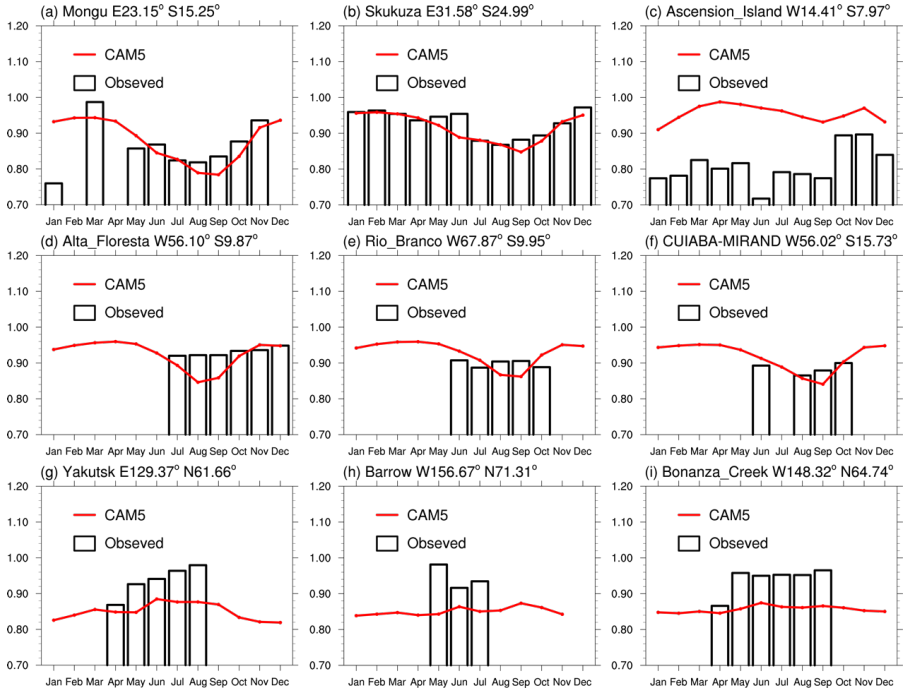

Figure 4. Same as Figure 3, but for the comparison of single scattering albedo (SSA) at 550 nm.

Atmos. Chem. Phys. Discuss., doi:10.5194/acp-2016-167, 2016
Manuscript under review for journal Atmos. Chem. Phys.
Published: 1 April 2016

Atmospheric Chemistry and Physics
Discussions

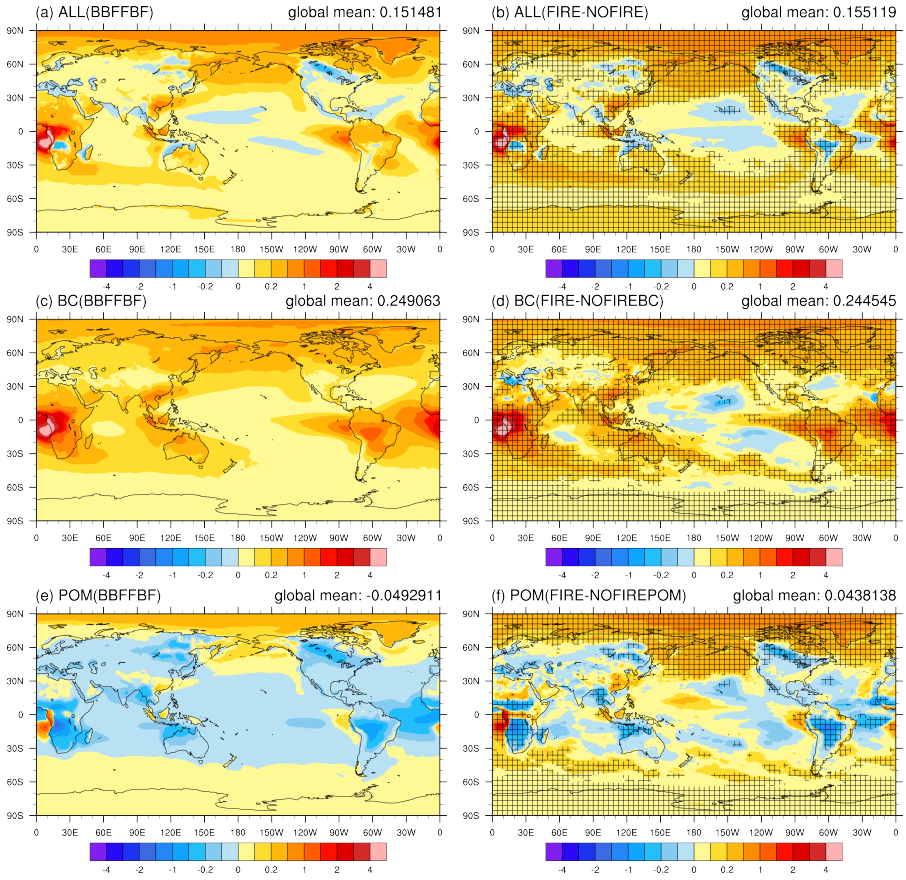

Figure 5. Annual mean direct radiative effect (DRE) (W m^{-2}) averaged over the period of 2003-2011 due to (a) all fire aerosols, (c) fire BC, and (e) fire POM estimated with the method of BBFFBF (left panels), and with the method of Ghan [2013] ((b), (d), and (f) in the right panels). The plus signs in Figure 5(b), (d) and (f) denote the regions where the radiative effect is statistically significant at the 0.05 level.

Atmos. Chem. Phys. Discuss., doi:10.5194/acp-2016-167, 2016
Manuscript under review for journal Atmos. Chem. Phys.
Published: 1 April 2016

Atmospheric Chemistry and Physics
Discussions

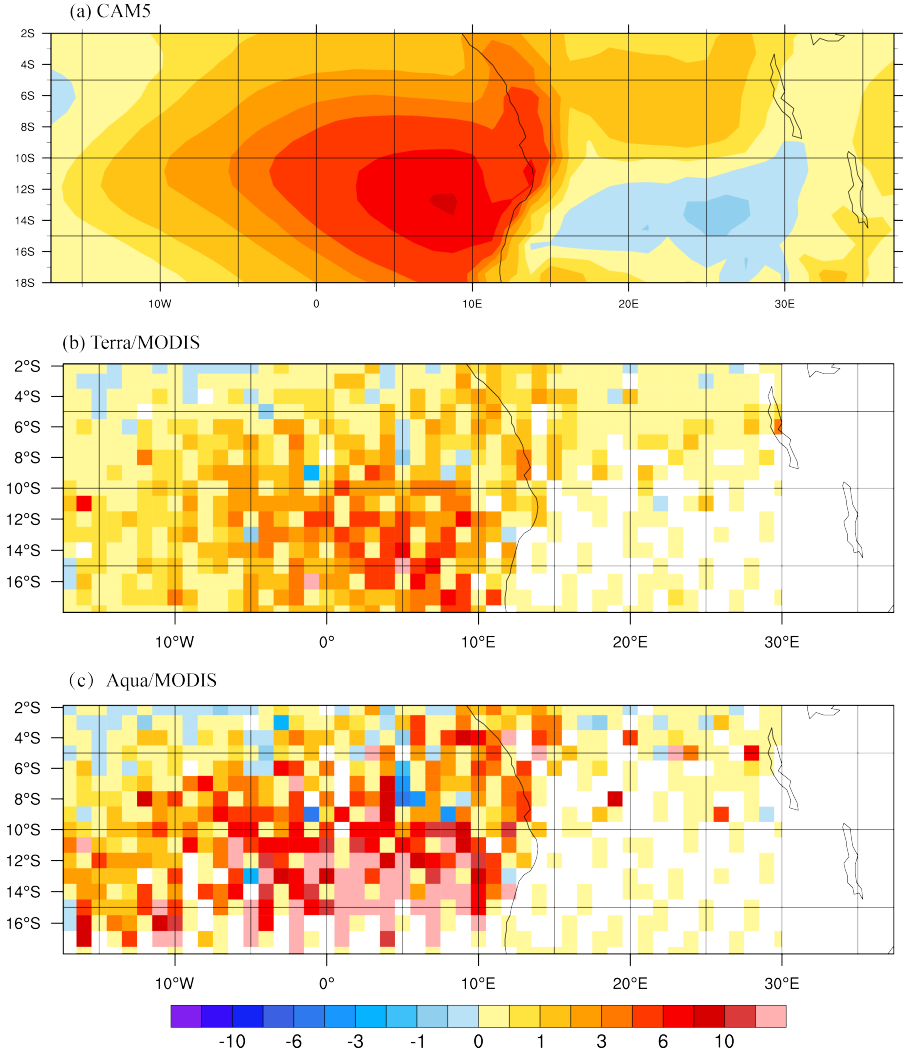

Figure 6. (a) September-October-November (SON) mean fire aerosol direct radiative effect (DRE) (W m^{-2}) for the period of 2003-2011 over the Southeast Atlantic Ocean due to all fire aerosols. (b) and (c) are the same as (a), but for the above-cloud aerosol DRE for the period of 2007-2011 estimated using Aqua/MODIS and Terra/MODIS products [*Zhang et al.*, 2014], respectively.

Atmos. Chem. Phys. Discuss., doi:10.5194/acp-2016-167, 2016
Manuscript under review for journal Atmos. Chem. Phys.
Published: 1 April 2016

Atmospheric Chemistry and Physics
Discussions

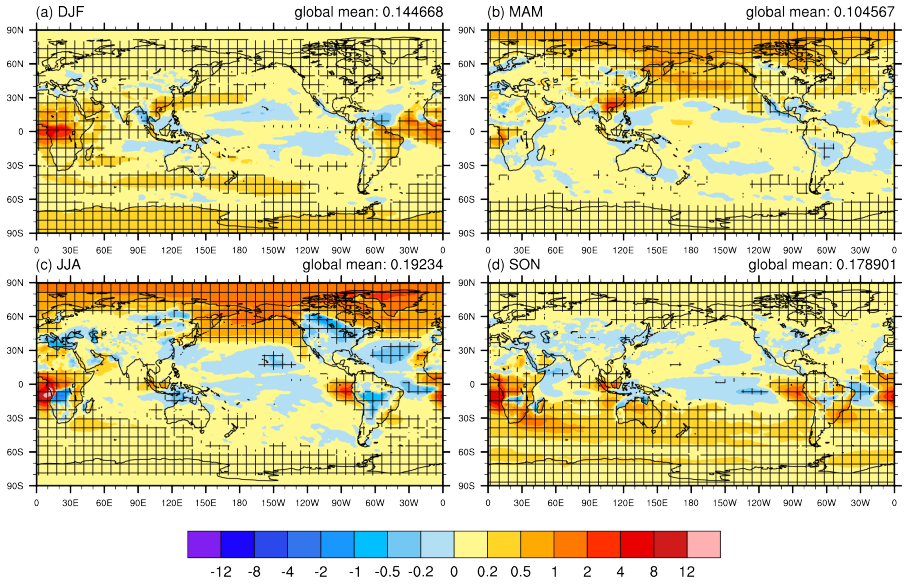

Figure 7. Direct radiative effect (DRE) (W m^{-2}) for the period of 2003-2011 due to all fire aerosols for (a) December-January-February (DJF), (b) March-April-May (MAM), (c) June-July-August (JJA), and (d) September-October-November (SON). The plus signs denote the regions where the DRE is statistically significant at the 0.05 level.

Atmos. Chem. Phys. Discuss., doi:10.5194/acp-2016-167, 2016
Manuscript under review for journal Atmos. Chem. Phys.
Published: 1 April 2016

Atmospheric Chemistry and Physics
Discussions

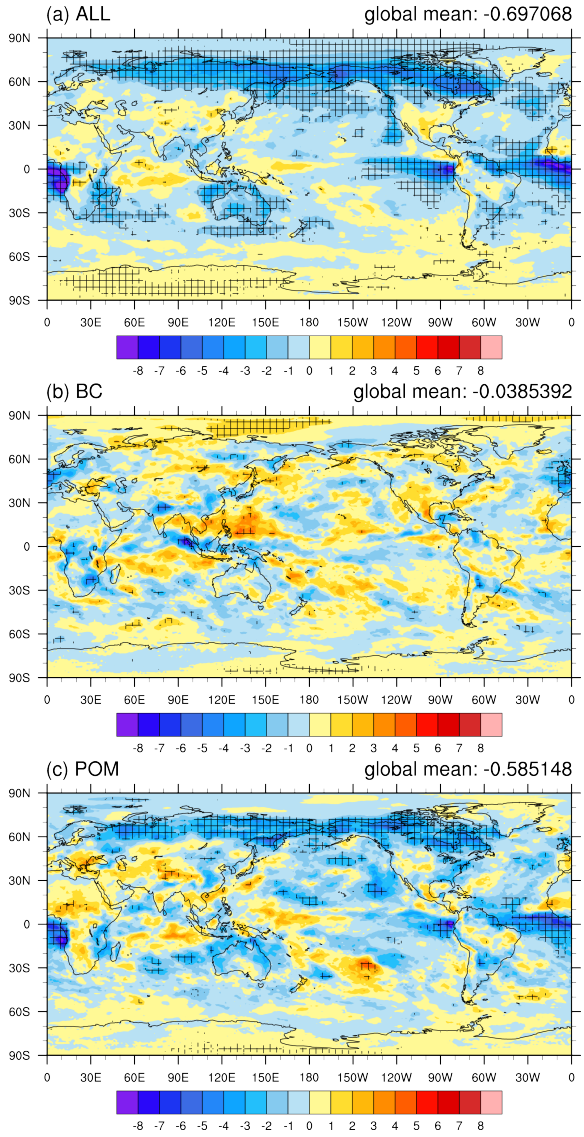

Figure 8. Annual mean cloud radiative effect (CRE) (W m^{-2}) averaged over the period of 2003-2011 due to (a) all fire aerosols, (b) fire BC, and (c) fire POM. The plus signs denote the regions where the radiative effect is statistically significant at the 0.1 level.

Atmos. Chem. Phys. Discuss., doi:10.5194/acp-2016-167, 2016
Manuscript under review for journal Atmos. Chem. Phys.
Published: 1 April 2016

Atmospheric Chemistry and Physics
Discussions

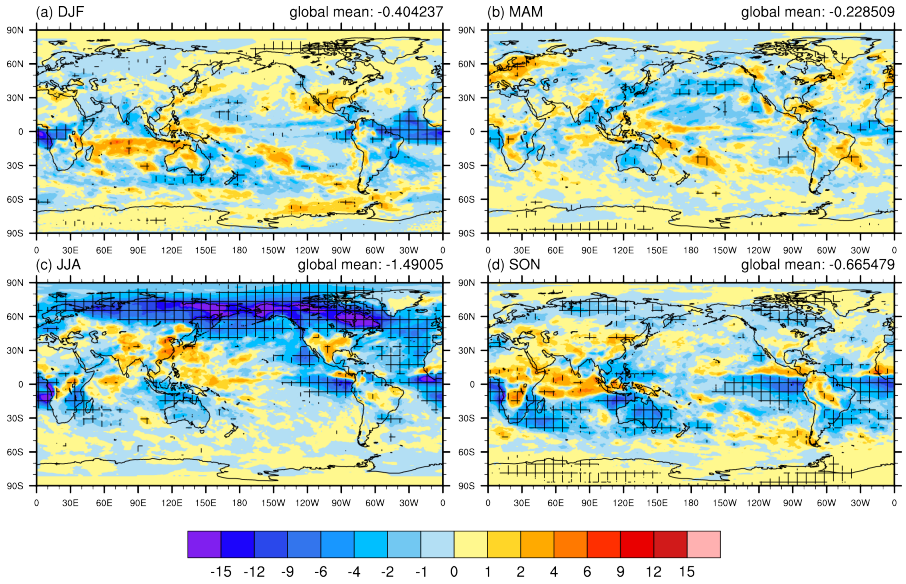

Figure 9. Seasonal variation of cloud radiative effect (CRE) (W m^{-2}) due to all fire aerosols for the period of 2003-2011 for (a) December-January-February (DJF), (b) March-April-May (MAM), (c) June-July-August (JJA), and (d) September-October-November (SON). The plus signs denote the regions where the CRE is statistically significant at the 0.05 level.

Atmos. Chem. Phys. Discuss., doi:10.5194/acp-2016-167, 2016
Manuscript under review for journal Atmos. Chem. Phys.
Published: 1 April 2016

Atmospheric Chemistry and Physics
Discussions

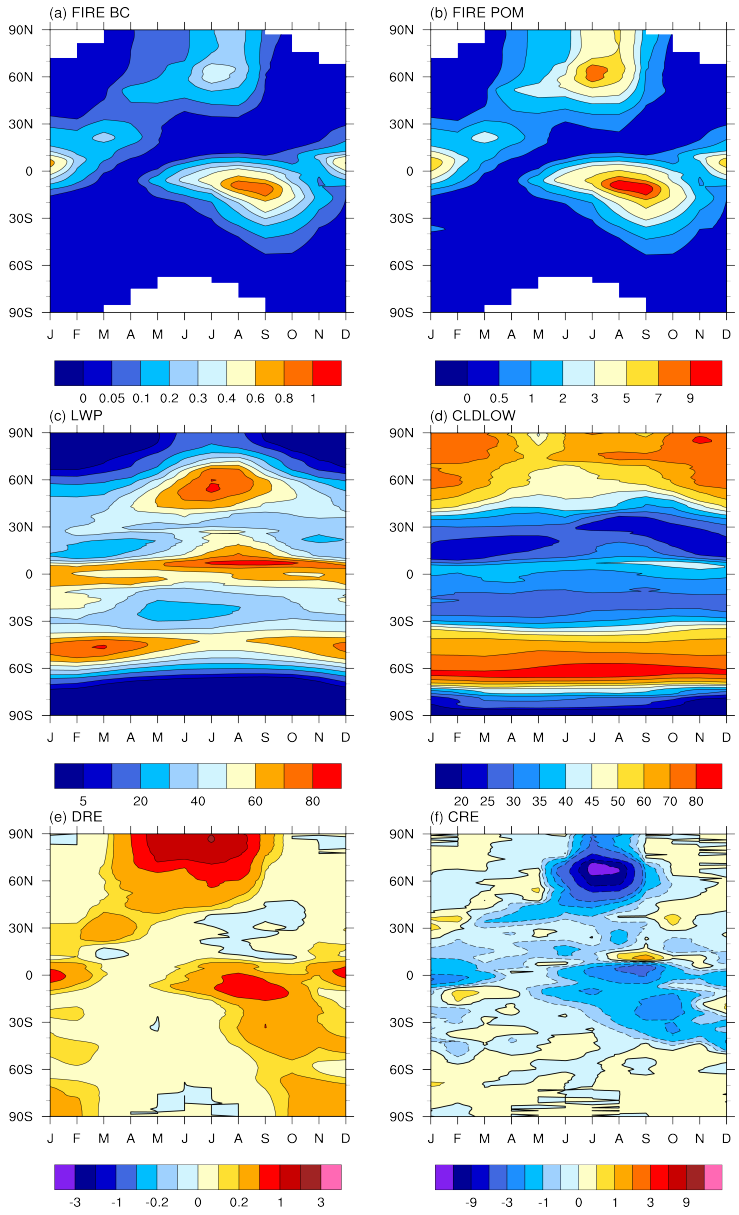

Figure 10. Month-latitude cross sections of zonal mean and monthly (a) vertically-integrated concentrations (mg m^{-2}) of fire BC and (b) fire POM, (c) cloud liquid water path (LWP, in g m^{-2}), (d) low-level cloud cover (CLDLOW, in %), (e) DRE (W m^{-2}), and (f) CRE (W m^{-2}) of fire aerosols.

Atmos. Chem. Phys. Discuss., doi:10.5194/acp-2016-167, 2016
Manuscript under review for journal Atmos. Chem. Phys.
Published: 1 April 2016

Atmospheric Chemistry and Physics
Discussions

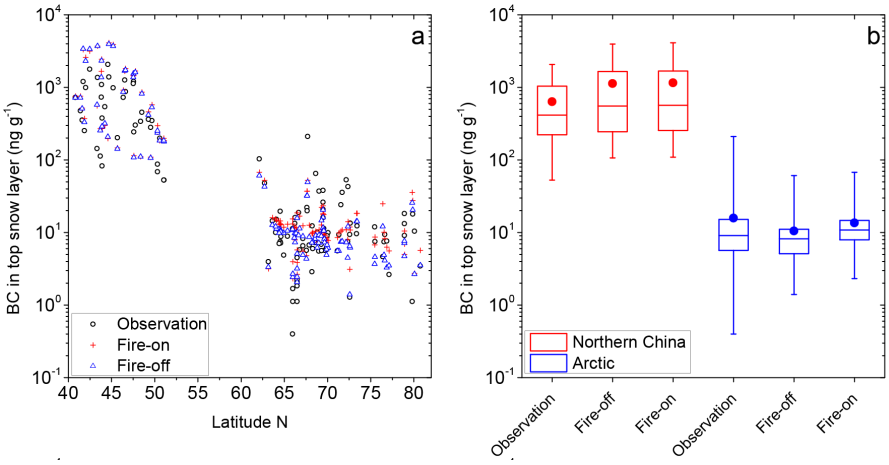

Figure 11. Evaluation of CAM5 simulated black carbon (BC) concentration for the period of 2003-2011 (in ng g^{-1}) in the top snow layer against observations in the Arctic (*Doherty et al.*, 2010) and Northern China (*Wang et al.*, 2013b). The top snow layer ranges in thickness from 1 to 3 cm. Configuration of the two CAM5 simulations (FIRE and NOFIRE) is summarized in Table 1. Panel (a) shows the comparisons at different latitudes. The box and whisker plot in panel (b) shows the minimum and maximum value with the bar, the 25th and 75th percentiles with the box, the 50th percentile (i.e., median) by the bar within the box, and the mean value with the dot.

Atmos. Chem. Phys. Discuss., doi:10.5194/acp-2016-167, 2016
Manuscript under review for journal Atmos. Chem. Phys.
Published: 1 April 2016

Atmospheric Chemistry and Physics
Discussions

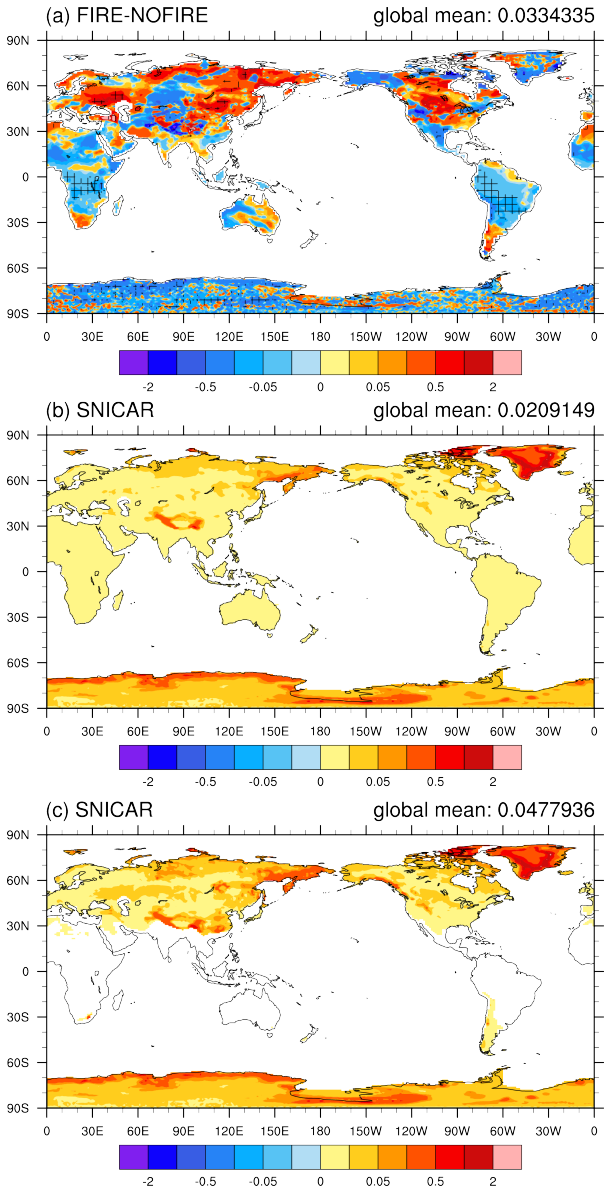

Figure 12. (a) Annual mean surface albedo effect (SAE, W m^{-2}) averaged over the period of 2003-2011 of all fire aerosols over land regions, and annual mean surface effect of fire BC-in-snow calculated from SNICAR averaged (b) over all times and (c) only when snow is present. The plus signs in (a) denote the regions where the radiative effect is statistically significant at the 0.1 level.

Atmos. Chem. Phys. Discuss., doi:10.5194/acp-2016-167, 2016
Manuscript under review for journal Atmos. Chem. Phys.
Published: 1 April 2016

Atmospheric Chemistry and Physics
Discussions

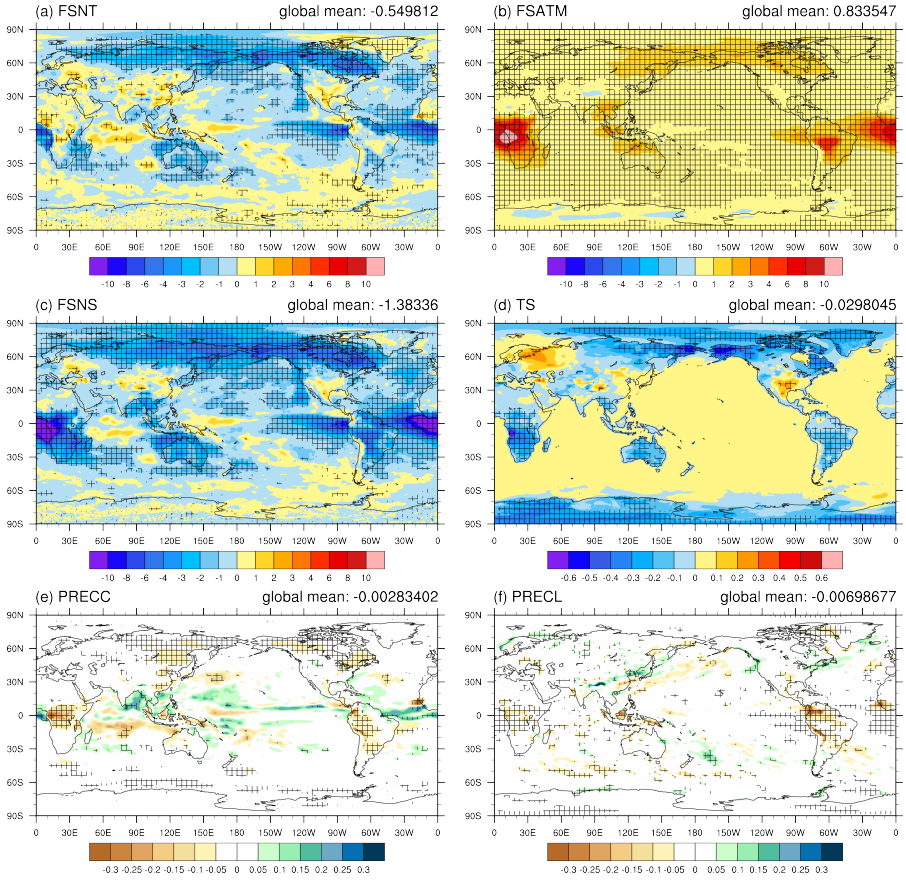

Figure 13. Annual mean net shortwave flux changes (W m^{-2}) over the period of 2003-2011 (a) at top of the atmosphere, (b) in the atmosphere, (c) at surface, and changes of (d) surface air temperature (K), (e) convective precipitation (mm d^{-1}), and (f) large-scale precipitation (mm d^{-1}) due to all fire aerosols. The plus signs denote the regions where the change is statistically significant at the 0.1 level.

Atmos. Chem. Phys. Discuss., doi:10.5194/acp-2016-167, 2016
Manuscript under review for journal Atmos. Chem. Phys.
Published: 1 April 2016

Atmospheric Chemistry and Physics
Discussions

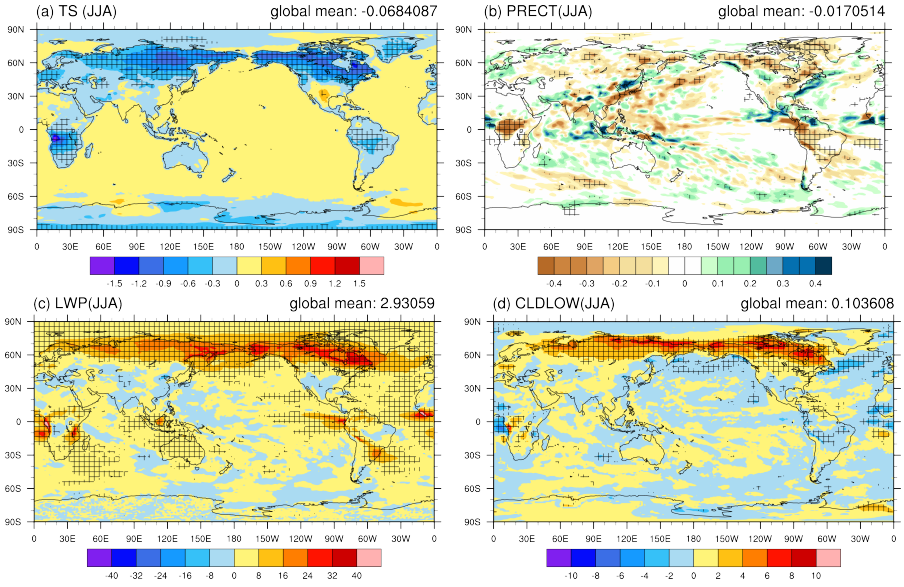

Figure 14. Changes in (a) surface air temperature (K), (b) total precipitation (mm d^{-1}), (c) cloud liquid water path (g m^{-2}), and (d) low-level cloud cover (%) due to all fire aerosols in the boreal summer (JJA) averaged for the period of 2003-2011. The plus signs denote the regions where the change is statistically significant at the 0.1 level.